Cell Reports

Article

MEG frequency tagging reveals a grid-like code during attentional movements

Graphical abstract

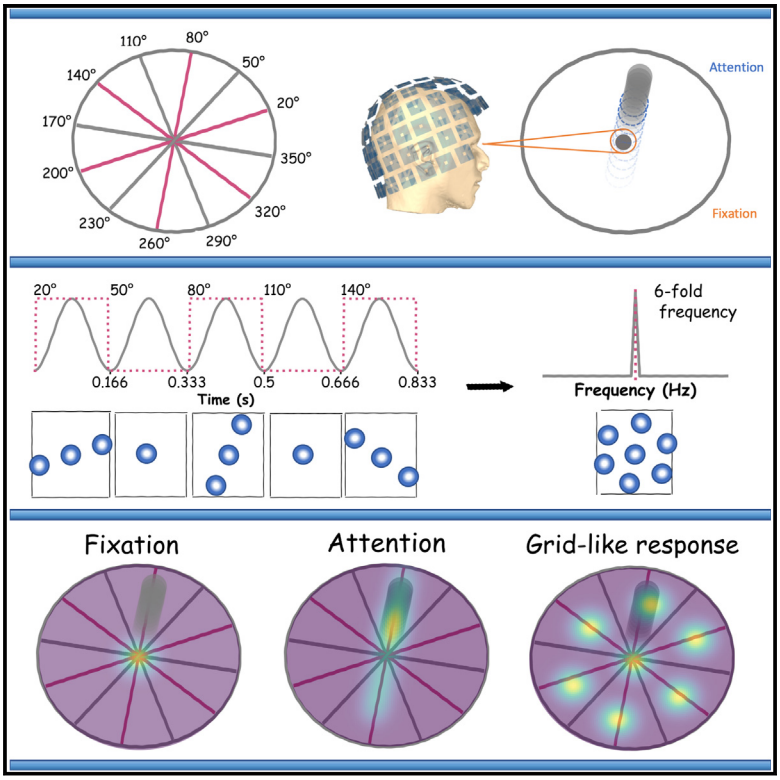

Highlights

- In humans, a grid-like response emerges during covert visual exploration
- Grid-like coding can be detected in MEG using a frequency-tagging paradigm
- Novel non-invasive method to investigate grid-like response in humans

Authors

Giuliano Giari, Lorenzo Vignali, Yangwen Xu, Roberto Bottini

Correspondence

giuliano.giari@unitn.it (G.G.), roberto.bottini@unitn.it (R.B.)

In brief

Giari et al. used MEG and frequency tagging to non-invasively investigate correlates of covert visual-space exploration in humans. A grid-like response was observed in the medial-temporal lobe and does not depend on the temporal structure of the task. Attentional mechanisms can account for navigation of abstract spaces.

Giari et al., 2023, Cell Reports *42*, 113209
October 31, 2023
https://doi.org/10.1016/j.celrep.2023.113209

Cell Reports

CellPress
OPEN ACCESS

Article

MEG frequency tagging reveals a grid-like code during attentional movements

Giuliano Giari,[1,*] Lorenzo Vignali,[1] Yangwen Xu,[1] and Roberto Bottini[1,2,*]
[1]Center for Mind/Brain Sciences (CIMeC), University of Trento, 38123 Trento, Italy
[2]Lead contact
*Correspondence: giuliano.giari@unitn.it (G.G.), roberto.bottini@unitn.it (R.B.)
https://doi.org/10.1016/j.celrep.2023.113209

SUMMARY

Grid-cells firing fields tile the environment with a 6-fold periodicity during both locomotion and visual exploration. Here, we tested, in humans, whether movements of covert attention elicit grid-like coding using frequency tagging. Participants observed visual trajectories presented sequentially at fixed rate, allowing different spatial periodicities (e.g., 4-, 6-, and 8-fold) to have corresponding temporal periodicities (e.g., 1, 1.5, and 2 Hz), thus resulting in distinct spectral responses. We found a higher response for the (grid-like) 6-fold periodicity and localized this effect in medial-temporal sources. In a control experiment featuring the same temporal periodicity but lacking spatial structure, the 6-fold effect did not emerge, suggesting its dependency on spatial movements of attention. We report evidence that grid-like signals in the human medial-temporal lobe can be elicited by covert attentional movements and suggest that attentional coding may provide a suitable mechanism to support the activation of cognitive maps during conceptual navigation.

INTRODUCTION

Understanding the surrounding environment is fundamental for animals' survival. To this end, sensory information is organized into so-called "cognitive maps," an internal model of the environment that supports flexible behavior.[1]

Cognitive maps are thought to be instantiated at the neural level through several neurons responding to spatial variables.[2] Among these, grid cells in the entorhinal cortex exhibit multiple firing fields that cover the navigable surface with a 60° rotational symmetry[3] (6-fold). The finding of spatially modulated cells has been pioneered in rodents, and comparable evidence has been reported in humans in virtual navigation tasks, with invasive direct neural recordings[4,5] but also using non-invasive functional magnetic resonance imaging (fMRI).[6]

Interestingly, in primates the neural mechanisms that evolved to support spatial exploration through locomotion seem to be recruited when space is explored through eye movements.[7,8] In non-human primates, grid cells exhibit their hexagonal firing also when space is explored through saccadic eye movements.[9,10] Similarly, Staudigl and colleagues[11] reported in humans a higher gamma-band power (60–120 Hz) in the medial-temporal lobe (MTL) for saccades aligned to the participants' grid. Moreover, grid-like responses in the human MTL have been reported using fMRI during visual search[12] and smooth pursuit.[13]

Findings of a grid-like response during visual exploration suggest the possibility of an attentional mechanism taking place.[14] Gaze position can be conceived as being the overt index of the currently attended location. Attention, however, can also be covertly deployed to peripheral spatial locations without moving the eyes.[15] Interestingly, a grid-like response in entorhinal cells has been reported in non-human primates trained to maintain central fixation while covertly paying attention to a dot moving in the periphery.[16] However, in humans there is no evidence of grid-like responses being dissociated from overt visual exploration of the environment.

We set out to investigate whether grid-like coding can be elicited, in humans, by movements of covert attention using frequency tagging (FT).[17,18] Following previous studies,[15,16] we defined covert attention as being the orientation of attention toward spatial locations achieved independently of directly observable eye movements. Instead of relying on currently established non-invasive methods to detect grid-like responses,[19] we developed a method that enables one to obtain an objective index of neural response that does not require participants' overt behavior.[17] In fact, FT relies on the brain's ability to track regularities embedded within a periodic presentation of stimuli, offering the advantage of measuring periodic neural responses with high signal-to-noise ratio.

Our FT method relied on rhythmic visual presentation of trajectories, appearing in fixed sequences of angles linearly spaced by either 15° or 30° in different trials (Figure 1A; Videos S1, S2, S3, and S4). This sequential "clock-like" presentation allowed to embed multiple spatial periodicities at different temporal intervals within the sequence. For instance, in the 30° resolution, trajectories separated by 60° (6-fold, i.e., grid-cell periodicity) appeared at 3 Hz, while trajectories separated by 90° (4-fold, control periodicity) appeared at 2 Hz. The aforementioned frequencies were thus "tagged" with different

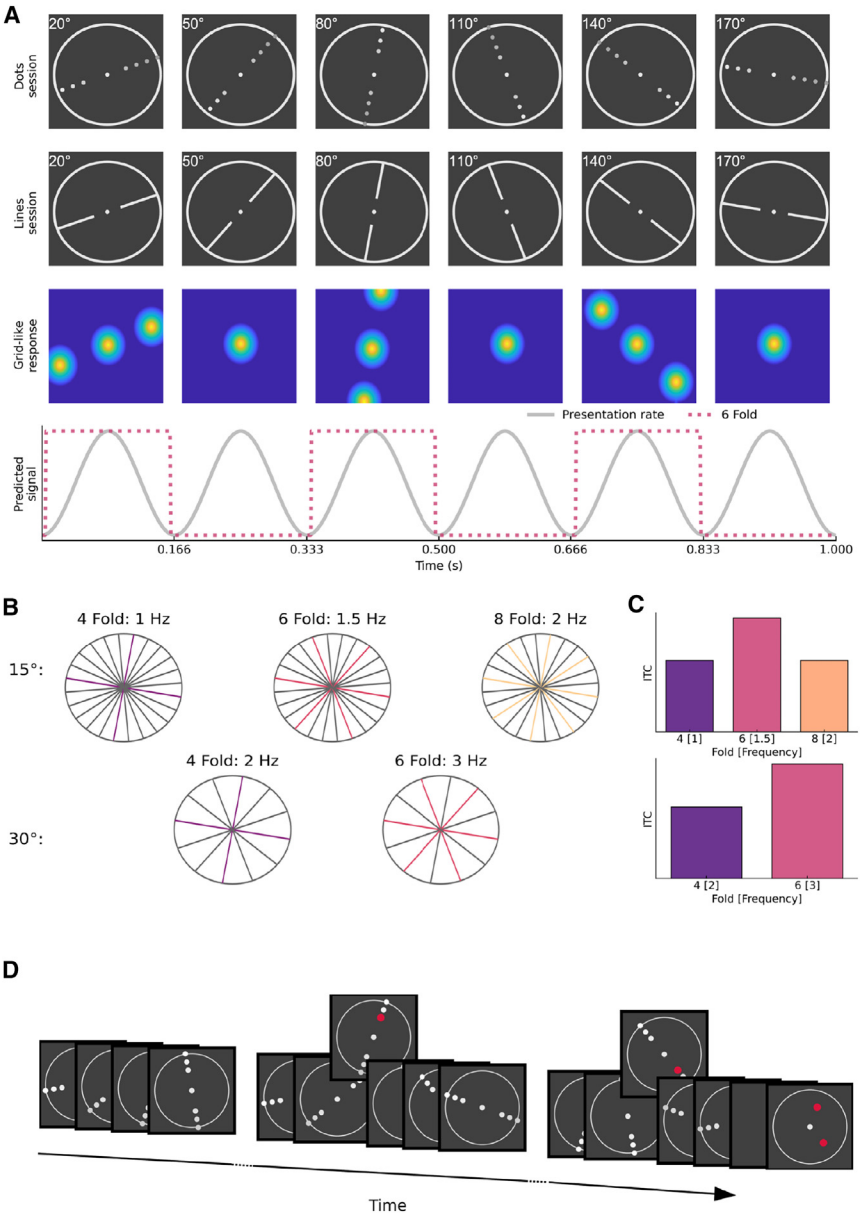

Figure 1. Frequency tagging design

(A) Example of a sequence at 30° resolution. Individual trajectories were presented continuously every 0.166 s (6 Hz). The same trajectories were presented in one session as dots moving from one side to the other of the circular arena (6 dots are shown here for visualization purposes; in the experiment 16 dots were presented) and in another session as static lines. Crucially, within this sequential presentation were embedded additional spatial regularities. For instance, trajectories separated by 60° (6-fold) appear every 0.333 s (3 Hz). See Videos S1–S4 for examples of trials of the different sessions and of the different angular resolutions.

(B) Multiple spatial regularities can be embedded within the sequential presentation of linearly spaced trajectories. Specifically, spatial regularities embedded in the 15° resolution include 90° (4-fold, purple) appearing every 1 s (1 Hz), 60° (6-fold, pink) appearing every 0.666 s (1.5 Hz), and 45° (8-fold, yellow) appearing every 0.5 s (2 Hz). The 30° resolution instead includes 4-fold appearing every 0.5 s (2 Hz) and 6-fold appearing every 0.333 s (3 Hz). The 6-fold periodicity corresponds to the grid-like periodicity, whereas the others act as control periodicities. Having two angular resolutions allows to "tag" different frequencies with the same spatial periodicity: 6-fold trajectories occur at 3 Hz in the 30° resolution and at 1.5 Hz in the 15° resolution, enabling an estimation of the neural tracking that is not tied to a specific chosen frequency.

(C) Predictions. If the spatial regularities were being tracked, a response at the corresponding frequency would be visible in the frequency spectrum. Isolating the frequencies of interest should then reveal a higher neural tracking for the frequency tagged with 6-fold (pink) as compared to 4-fold (purple) and 8-fold (yellow) in the 15° resolution (top) as well as a higher response for the frequency tagged with 6-fold as compared to 4-fold in the 30° resolution (bottom).

(D) Task. During the trajectories' sequence (both sessions) two red dots appeared for 0.025 s in random locations along the trajectory. To ensure spatial attention, timing of their appearance was randomized but constrained between 19 s and 33 s for the first dot and between 37 s and 39 s for the second dot. At the end of the trial, two red dots were presented again and participants had to indicate whether their position was consistent with the one they were keeping in memory.

spatial periodicities (Figure 1B). If any of these regularities were being tracked, a response at the corresponding frequency would emerge in the magnetoencephalography (MEG) signal (Figure 1C). Compared to current non-invasive methods, the recurrent presentation of 6-fold regularities avoids the need to estimate the grid orientation with the maximal periodic response. A peak at the frequency corresponding to the presentation of 6-fold trajectories is itself an index that during the stimulation there was a successful recognition of a 6-fold periodicity in the trajectories' presentation. Crucially, this FT measure does not depend on the participant-specific preferred orientation: the same frequency response should be observed if the grid is aligned to any of the trajectories in the sequence. In fact, the continuous clock-like presentation allows a consistent temporal interval between the preferred trajectory (i.e., orientation) and its 60° multiples, irrespective of the participant-specific orientation.

We recorded MEG and eye tracking while participants attended to the FT presentation. We quantified the neural tracking of the spatial periodicities using inter-trial coherence (ITC)[20] and observed a grid-like response: the frequency tagged with the 6-fold periodicity shows higher ITC than control periodicities.

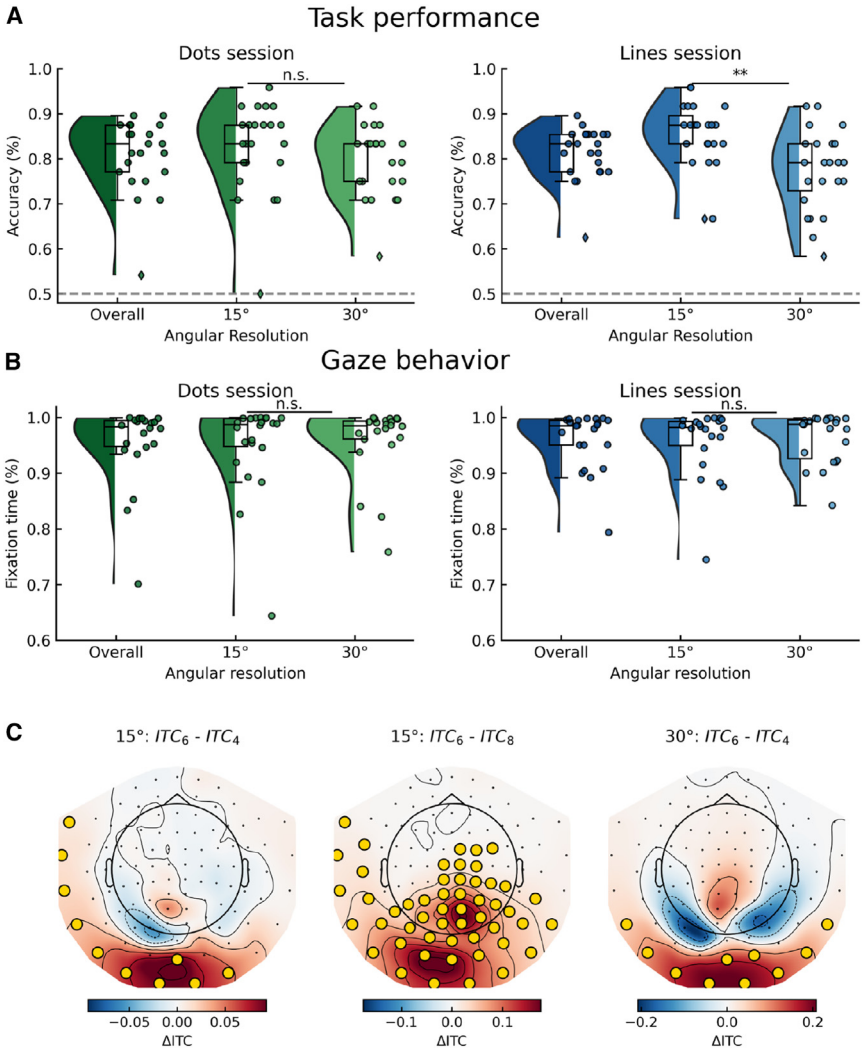

Figure 2. Covert tracking of spatial trajectories elicited a grid-like response detectable with frequency tagging

(A) Accuracy in the location memory task, averaged over angular resolutions as well as separately for each angular resolution. Performance was overall good (dots session: mean = 80%, SD = 7%; lines session: mean = 81%, SD = 5%) except for one participant (diamond point in the plot) whose accuracy (dots: 54%; lines: 62%) was two SDs below group mean in both sessions. This participant was excluded from further analyses. After separating the responses in the two angular resolutions, we observed higher accuracy in the 15° resolution ($t(22) = 3.18$, $p = 0.004$) in the lines session, while no difference was observed in the dots session ($t(22) = 1.71$, $p = 0.099$).

(B) Fixation time during the trials, expressed as percentage, averaged over angular resolutions as well as separately for each angular resolution. Participants kept central fixation (4.5° visual angle from the center of the screen[16]) for the majority of the time during the trial. No differences in fixation behavior were found between angular resolutions (dots session: $t(21) = -1.06$, $p = 0.300$; lines session: $t(21) = -1.16$, $p = 0.257$). Green shades indicate dots session, blue shades indicate lines session. Lines above data points indicate significance (n.s., not significant; *$p < 0.05$; **$p < 0.01$; ***$p < 0.001$).

(C) Significant clusters at sensor level in which ITC_6 is greater than control ITCs, indicating a grid-like response in occipito-temporal sensors. In the 15° resolution, ITC_6 is greater than ITC_4 ($p = 0.038$ cluster corrected, left) and ITC_6 is greater than ITC_8 ($p < 0.001$ cluster corrected, center). In the 30° resolution, ITC_6 is greater than ITC_4 ($p = 0.047$ cluster corrected, right). No clusters were found in which control periodicities were higher than 6-fold periodicity.

See Figures S1 and S2 for results of the individual sessions.

At sensor level this effect was found in clusters encompassing occipital and temporal sensors, whereas at source level this effect was found specifically in the MTL. Concurrently recorded gaze location and participants' accurate performance allowed us to ascribe the observed effect to covert attention. In a control experiment we used the same FT design with non-spatially structured stimuli. We observed a different response profile, indicating the dependency of the effect observed in the spatial experiment on covert movements of attention.

RESULTS

Participants were covertly tracking the spatial trajectories

Twenty-three healthy volunteers completed two MEG recording sessions. In one session, trajectories were formed by dots moving from one side to the other in a circular arena, similar to the method used by Nau et al.[13] In another session, the same trajectories were presented as static lines. Participants were instructed to fixate at the center of a screen while attending to the trajectories. To ensure they were paying attention to the stimuli, they were asked to perform a location memory task (Figure 1D). This consisted of two red dots appearing at random positions along the trajectories and at random times within the trial sequence. Participants had to remember the dot's exact position, and their memory was tested at the end of each trial. Performance overall was accurate (Figure 2A), except for one participant that was excluded from further analyses.

Gaze-location data confirmed that participants were keeping central fixation (4.5° visual angle[16]) throughout the trial (Figure 2B). To further make sure that any MEG response can be ascribed to covert attention, trials in which fixation was maintained for less than 80% of the time were excluded from further analyses. This threshold was used during the recording session to warn participants of excessive eye movements and was thus kept during the analysis stage, but the main findings are replicated using a more stringent threshold of 95% of time (Figure S4).

Taken together, participants' behavior as reflected in task performance and gaze position indicates successful covert tracking of the spatial trajectories.

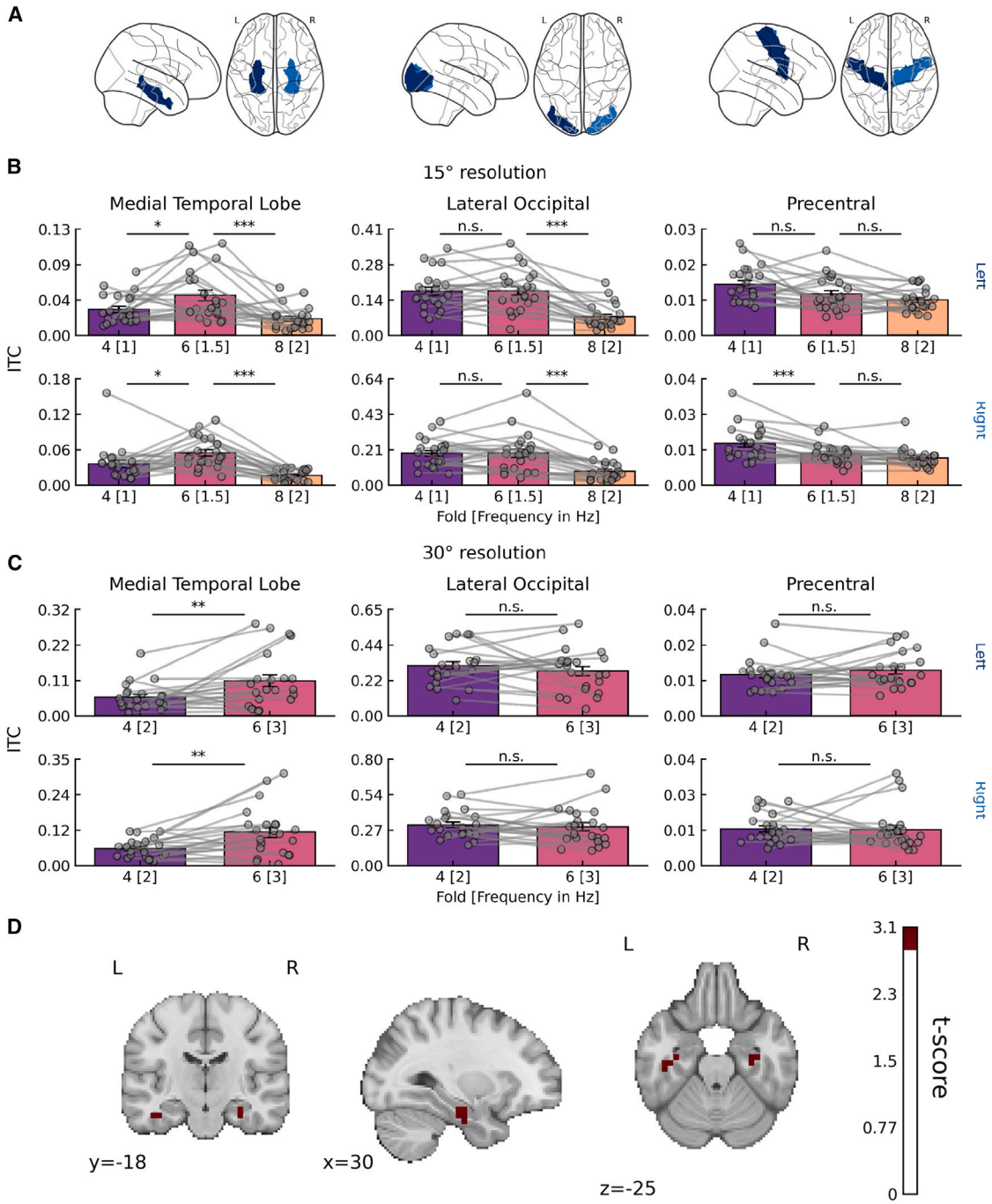

Figure 3. Grid-like response during covert attention originated in the MTL

(A) Regions of interest (ROIs) selected for the source-level analyses. From left to right: medial-temporal lobe (MTL; hippocampus, entorhinal, and parahippocampal cortices), lateral occipital, and precentral. Dark blue indicates left hemisphere and light blue indicates right hemisphere.

(B) Inter-trial coherence (ITC) in the ROIs for each frequency tagged with spatial periodicities at 15° resolution demonstrate the presence of a grid-like response, i.e., the frequency tagged with the 6-fold spatial periodicity (pink) was higher than both control periodicities (4-fold: purple; 8-fold: yellow) in the MTL (left) in both the left hemisphere (top) and right hemisphere (bottom). The grid-like effect was specific to the MTL in that in neither the lateral occipital (center) nor precentral (right) control ROI was the 6-fold periodicity higher than both control periodicities.

(C) ITC in the ROIs for each for each frequency tagged with spatial periodicities at 30° resolution demonstrate the presence of a grid-like response in the MTL ROI (left) in both the left (top) and right (bottom) hemisphere, with the 6-fold periodicity (pink) being higher than the 4-fold periodicity (purple). This effect was specific to

(legend continued on next page)

MEG FT detects a grid-like response in humans during covert attentional movements

As a first step, we sought to understand whether the FT method was able to detect a grid-like response by quantifying the neural tracking of the spatial periodicities with ITC at sensor level. This analysis is based on the signal as recorded by MEG but will provide limited spatial information. After standard MEG preprocessing, the time series of each trial was divided into shorter segments, which then underwent a semi-automatic artifact rejection procedure (see STAR Methods). Individual segments were decomposed in the frequency domain with a fast Fourier transform (FFT), and this complex representation was used to calculate ITC following previous studies.[21,22] Having observed no statistical differences in the ITC response between the dots and lines sessions in the predicted source-level region of interest (ROI) analysis, we averaged the results and carried out our main analyses on this averaged ITC value (see "grid-like response was localized in medial-temporal sources" for the formal comparison and Figures S1 and S2 for the individual session results).

The ITC of the frequencies corresponding to the 6-fold periodicity (ITC_6) was compared to the ITC at the frequency of the control periodicities (ITC_4 and ITC_8) with a two-sided cluster-permutation test,[23] separately for each angular resolution. For the sensor-level analysis we focused on magnetometers, given their higher sensitivity to deep sources as compared to gradiometers.[24] This analysis revealed significant clusters encompassing occipital and temporal sensors in which ITC_6 was higher than the control periodicities (Figure 2C). Specifically, in the 15° resolution we observed a cluster in which ITC_6 was greater than ITC_4 ($p = 0.038$ cluster corrected) and a cluster in which ITC_6 was greater than ITC_8 ($p < 0.001$ cluster corrected). In the 30° resolution, we observed a cluster in which ITC_6 was greater than ITC_4 ($p = 0.047$ cluster corrected). No cluster was found in which control periodicities' ITCs were greater than ITC_6.

This analysis indicates that covert attentional movements in humans also elicit a grid-like response, similarly to non-human primates.[16] The limited spatial resolution of sensor-level analyses localized this response in occipito-temporal sensors, with similar topographies giving rise to the grid-like effect in both angular resolutions (Figure S10B).

Grid-like response was localized in medial-temporal sources

We performed source localization to investigate which brain areas were responsible for the grid-like effect observed at sensor level. We used a linearly constrained minimum variance beamformer[25] to reconstruct the time series of brain activity in each voxel and computed the ITC at the frequencies corresponding to the tagged spatial periodicities (see STAR Methods).

We focused our analysis on the MTL (Figure 3A, left), given the a priori hypothesis of its involvement in the generation of the 6-fold periodic response. The average ITC value in this ROI was compared across sessions with a two-way repeated-measures analysis of variance (ANOVA) with factors session (dots, lines) and periodicity (15° resolution: 4-, 6-, 8-fold; 30° resolution: 4-, 6-fold) to evaluate whether the neural tracking of the spatial periodicities is elicited differently by moving dots or static lines. This analysis was repeated for each hemisphere and each angular resolution. We found no significant periodicity × session interaction (15°: left, $F(2,42) = 2.42$, $p = 0.101$; right, $F(2,42) = 1.44$, $p = 0.248$; 30°: left, $F(1,21) = 1.40$, $p = 0.25$; right, $F(1,21) = 0.19$, $p = 0.66$). The ITC values of the two sessions (dots and lines) were thus averaged together and used for further analyses (see Figures S1 and S2 for the individual session results).

Most interestingly, the ANOVA identified a main effect of periodicity in both hemispheres, and in both the 15° resolution (left: $F(2,42) = 9.27$, $p < 0.001$; right: $F(2,42) = 16.46$, $p < 0.001$; Figure 3B, left) and 30° (left: $F(1,21) = 8.63$, $p = 0.008$; right $F(1,21) = 11.89$, $p = 0.002$; Figure 3C, left). Planned paired t test indicated that in the 15° resolution, ITC_6 was significantly greater than both ITC_4 and ITC_8 in both hemispheres (Table 1). In the 30° resolution, ITC_6 was significantly greater than ITC_4 in both the left and right MTL (Table 1). Taken together, these results suggest the presence of a grid-like response in the MTL during covert attentional movements.

To investigate whether the grid-like effect was specific to the MTL, we compared the MTL with two control ROIs, the lateral occipital and precentral cortices (Figure 3A, center and right). We conducted a two-way repeated-measures ANOVA with factors ROI (MTL, lateral occipital, precentral) and periodicity (15° resolution: 4-, 6-, 8-fold; 30° resolution: 4-, 6-fold) separately for each hemisphere and each angular resolution. We found a significant two-way interaction in the 15° resolution (Figure 3B) in both the left hemisphere ($F(2.51, 52.75) = 29.62$, $p < 0.001$) and right hemisphere ($F(2.17, 45.66) = 20.82$, $p < 0.001$). Post hoc t test indicated that the effect was indeed specific to the MTL, as in neither the lateral occipital nor the precentral ROI was ITC_6 greater than both control periodicities (Table 1). In the 30° resolution (Figure 3C) we observed a significant two-way interaction in the left hemisphere ($F(1.35, 28.27) = 4.94$, $p = 0.025$) and the right hemisphere ($F(1.39, 29.13) = 4.79$, $p = 0.026$). Post hoc t tests confirmed that in the control regions ITC_6 was not greater than both control periodicities (Table 1).

To localize this effect at the cortical level, we performed a conjunction analysis.[26] This analysis revealed clusters of voxels in the bilateral MTL that survived an uncorrected threshold ($p < 0.005$) (Figure 3D). In addition, a cluster-permutation test at the cortical level identified significant clusters encompassing the MTL in both 15° and 30° resolution (Figure S3).

Given their higher sensitivity to deep sources,[24] we also repeated source analysis using only magnetometers. We did not find differences from the main results reported above (Figure S5).

the MTL in that neither the lateral occipital nor precentral ROI show a comparable periodicity preference. Gray dots indicate individual subjects. Error bars indicate standard error of the mean. Lines above data points indicate significance (n.s., not significant; *$p < 0.05$; **$p < 0.01$; ***$p < 0.001$).

(D) Conjunction analysis (15°: $ITC_6 > ITC_4$ and $ITC_6 > ITC_8$; 30°: $ITC_6 > ITC_4$) at the cortical level ($p < 0.005$ uncorrected) demonstrated the specificity to the MTL of the grid-like effect.

See Figures S1 and S2 for results of the individual sessions.

Table 1. Pairwise comparison between tagged frequencies in the different ROIs in the spatial experiment

Angular resolution	Hemisphere	ROI	Comparison	df	t	p	Significance
15°	left	MTL	6-fold (1.5 Hz) vs. 4-fold (1 Hz)	21	2.35	0.028	*
			6-fold (1.5 Hz) vs. 8-fold (2 Hz)	21	3.92	<0.001	***
		lat. occipital	6-fold (1.5 Hz) vs. 4-fold (1 Hz)	21	0.07	0.937	
			6-fold (1.5 Hz) vs. 8-fold (2 Hz)	21	6.43	<0.001	***
		precentral	6-fold (1.5 Hz) vs. 4-fold (1 Hz)	21	−1.93	0.066	
			6-fold (1.5 Hz) vs. 8-fold (2 Hz)	21	1.83	0.08	
	right	MTL	6-fold (1.5 Hz) vs. 4-fold (1 Hz)	21	2.45	0.022	*
			6-fold (1.5 Hz) vs. 8-fold (2 Hz)	21	6.80	<0.001	***
		lat. occipital	6-fold (1.5 Hz) vs. 4-fold (1 Hz)	21	0.06	0.949	
			6-fold (1.5 Hz) vs. 8-fold (2 Hz)	21	6.09	<0.001	***
		precentral	6-fold (1.5 Hz) vs. 4-fold (1 Hz)	21	−4.15	<0.001	***
			6-fold (1.5 Hz) vs. 8-fold (2 Hz)	21	1.82	0.081	
30°	left	MTL	6-fold (3 Hz) vs. 4-fold (2 Hz)	21	2.92	0.008	**
		lat. occipital	6-fold (3 Hz) vs. 4-fold (2 Hz)	21	−1.01	0.322	
		precentral	6-fold (3 Hz) vs. 4-fold (2 Hz)	21	1.07	0.294	
	right	MTL	6-fold (3 Hz) vs. 4-fold (2 Hz)	21	3.43	0.002	**
		lat. occipital	6-fold (3 Hz) vs. 4-fold (2 Hz)	21	−0.39	0.698	
		precentral	6-fold (3 Hz) vs. 4-fold (2 Hz)	21	−0.14	0.884	

Post hoc t tests at source level in each ROI identified a significantly higher ITC_6 as compared to control folds in the 15° resolution in both the left and right MTL. The same pattern was not present in the control regions. Similarly, in the 30° resolution ITC_6 was higher than ITC_4, specifically in the MTL. Asterisks indicate significance: *p < 0.05; **p < 0.01; ***p < 0.001.

These results confirm that the grid-like response elicited by covert attentional movements originated in the MTL and was not present in control regions.

Gaze location does not influence the grid-like response

We then conducted further analyses on the eye-tracker data to investigate the presence of eye movements within the fixation window that could be induced by the presentation of the stimuli and their potential relation with the observed grid-like response.

First, we replicated the analysis conducted by Wilming and colleagues[16] to directly assess the time-resolved consistency between gaze location and stimuli position (Figure 4A). We separately computed the Euclidean distance of the eyes to the center and of the stimuli (dots) to the center at each time point. These distance measures would be correlated if the eyes were following the dots. However, at the group level we did not observe any correlation, neither in 15° ($t(21) = -1.169$, $p = 0.255$) nor in the 30° resolution ($t(21) = -0.814$, $p = 0.424$). Moreover, no difference was present between the 15° and 30° resolutions ($t(21) = -0.409$, $p = 0.686$). Thus, at least according to the standards adopted by Wilming and colleagues, attentional tracking during the task was not accompanied by consistent eye movements (at least in the case of the moving dot session, to which this kind of analysis could be applied). Moreover, by comparing the eye position in the moments directly before and after the appearance of the target dots, we found that the presentation of the target did not induce a consistent shift of gaze location (Figure S6), indicating that task-relevant stimuli were not influencing gaze behavior.

We then directly assessed the similarity between gaze locations during the presentation of different trajectories in both the dots and lines sessions. We used Gaussian kernel density estimate to calculate the heatmaps of fixations[27] for each trajectory, focusing on the predefined 4.5° × 4.5° fixation window (Figure 4B). The average pairwise correlations between the heatmaps were very high overall (dots session: 15°, $r = 0.97 \pm 0.01$; 30°, $r = 0.98 \pm 0.005$; lines session: 15°, $r = 0.97 \pm 0.01$; 30°, $r = 0.98 \pm 0.005$; Figure 4C), indicating that individual participants' gaze location was similar across trajectories.

However, despite the high similarity, we found that fixation maps of trajectories that were similar to each other were negatively correlated with the angular difference between trajectories (Figure 4D). Fisher-transformed r scores were significantly different from zero (dots session: 15°: $r = 0.71 \pm 0.09$, $t(21) = -20.232$, $p < 0.001$; 30°: $r = 0.82 \pm 0.064$, $t(21) = -26.486$, $p < 0.001$; lines session: 15°: $r = 0.69 \pm 0.08$, $t(21) = -25.224$, $p < 0.001$; 30°: $r = 0.81 \pm 0.05$, $t(21) = -32.202$, $p < 0.001$), indicating that individual participants' fixation similarity was (slightly) higher for trajectories that had smaller angular difference.

Given that the spatial trajectories induced a small but consistent bias in participants' gaze location, we next investigated whether this effect could influence the observed grid-like response. To this end we computed the slope of the correlation from the previous analysis and averaged it across sessions. This measure was taken as an index of the extent to which an individual participant's gaze was modulated by the angular difference between the trajectories. We then computed the slope of the grid-like effect in the left and right MTL, separately for each angular resolution: for the 15° resolution we fit a quadratic model centered on 6-fold to individual participants' ITC data in the MTL (see Figure 6 for similar analysis at the group level), while for the 30° resolution we fit a linear model. The slope of each model was taken as an index of the strength of the grid-like response. We

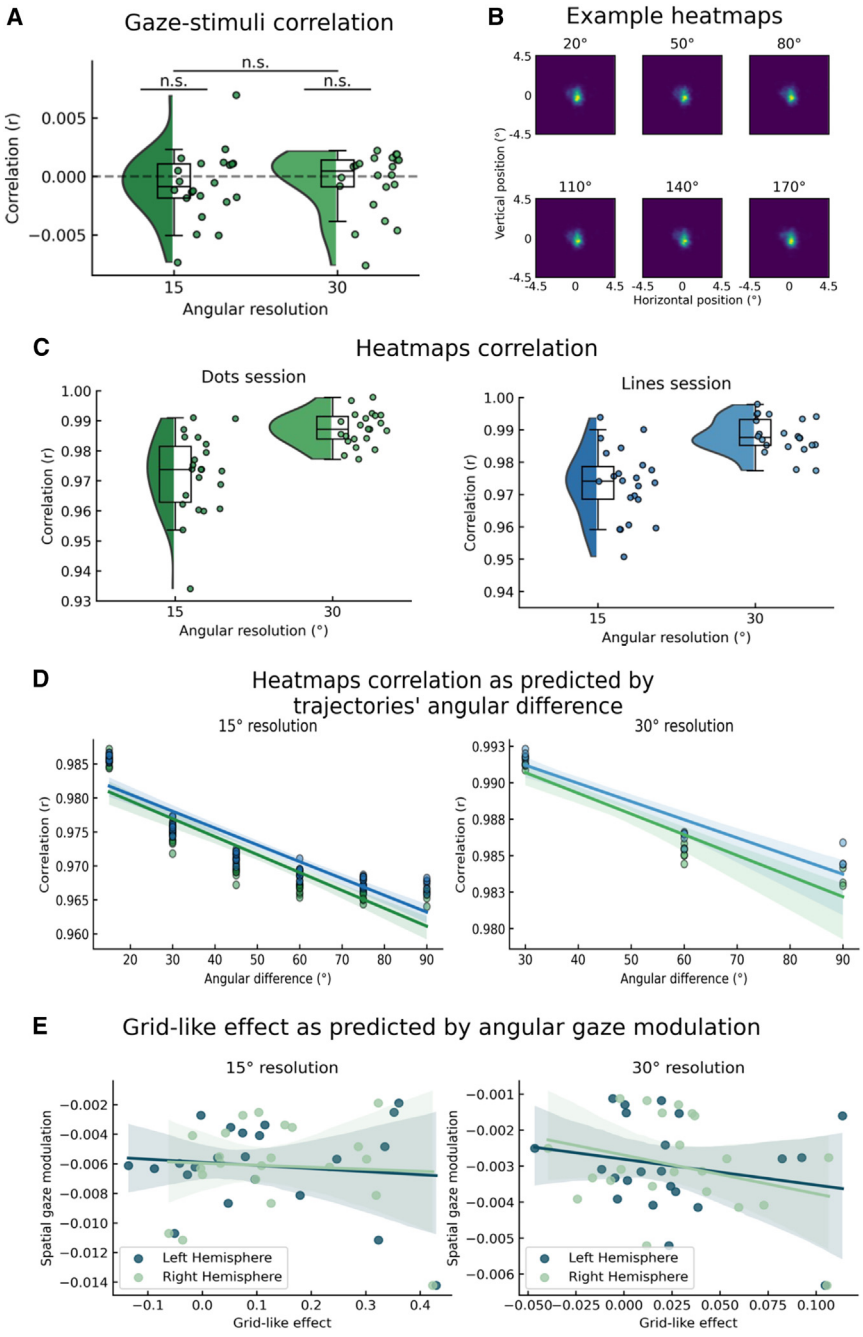

Figure 4. Gaze location does not influence the grid-like response

(A) Correlation across time between Euclidean distance of the eye to the center and the dot to the center, replicating the analysis conducted by Wilming and colleagues.[16] We did not observe any correlation at the group level, neither in 15° ($t(21) = -1.169$, $p = 0.255$) nor in 30° resolution ($t(21) = -0.814$, $p = 0.424$), and no difference was observed between the two angular resolutions ($t(21) = -0.409$, $p = 0.686$).

(B) Heatmaps (restricted to the fixation window) from one example participant for each trajectory in the 30° resolution.

(C) Average pairwise correlation (within-subject) between trajectory-specific heatmaps. Correlations were overall high in both the dots (green) and lines (blue) session.

(D) Group-average correlation as a function of angular difference for both the dots (green) and lines (blue) sessions, in both 15° (left) and 30° (right) resolution. We observed a significant negative correlation in all cases (dots session: 15°: $r = 0.71 \pm 0.09$, $t(21) = -20.232$, $p < 0.001$; 30°: $r = 0.82 \pm 0.064$, $t(21) = -26.486$, $p < 0.001$; lines session: 15°: $r = 0.69 \pm 0.08$, $t(21) = -25.224$, $p < 0.001$; 30°: $r = 0.81 \pm 0.05$, $t(21) = -32.202$, $p < 0.001$), indicating that trajectories with higher correlation were close in angular space.

(E) Grid-like effect as a function of the angular gaze modulation. The slope of the grid-like effect in each hemisphere was correlated with the slope of the correlation between the pairs of heatmaps and their angular difference. We found no correlation in either hemisphere and in neither the 15° (left) nor 30° resolution (right) (all $p > 0.172$).

See Figure S7 for the same analyses using gaze angle.

then correlated the slopes of the MEG and eye-tracker effects to investigate whether the participants that exhibited the strongest grid-like effect were also exhibiting a high modulation of the fixation pattern by the trajectories' presentation. We did not find any correlation (Figure 4E) in neither 15° (left hemisphere: $r(20) = -0.11$, $p = 0.618$; right hemisphere: $r(20) = -0.06$, $p = 0.789$) or 30° resolution (left hemisphere: $r(20) = -0.22$, $p = 0.335$; right hemisphere: $r(20) = -0.30$, $p = 0.172$).

As an additional control, we replicated the previous results using the time-resolved gaze angle instead of the gaze location represented in the heatmaps (Figure S7), strengthening the observation of a lack of correlation between gaze behavior and the grid-like effect.

Taken together, these results indicate that the presented spatial trajectories induced a small but consistent bias in participants' gaze location. Although it is unclear to what extent this fixation bias reflects shifts of attention along the presented trajectories (see the control analysis inspired by Wilming et al.[16] and the lack of correlation with the magnitude of the 6-fold effect), we cannot completely rule out this possibility. Indeed, there is an ongoing debate regarding whether miniature eye movements are inherently linked to shifts in spatial attention and can be taken as an index of covert attention.[28–30] Nevertheless, grid-like coding seems to emerge in the absence of directly observable, overt oculomotor exploration of the visual environment, as previously reported in non-human primates.[16]

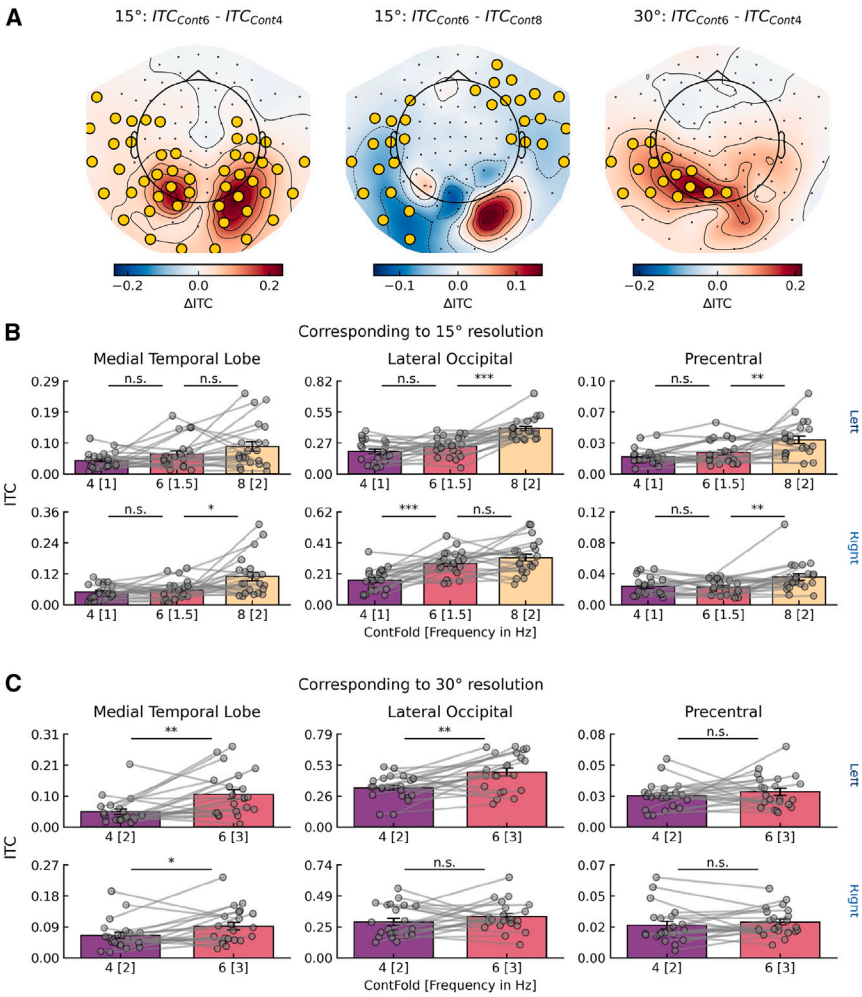

Figure 5. Temporal structure of the frequency-tagging design does not elicit a grid-like response

(A) Sensor-level clusters observed in the non-spatial experiment comparing the frequencies tagged with spatial periodicities in the spatial experiment. In the condition corresponding to 15°, ITC$_{Cont6}$ was greater than ITC$_{Cont4}$ ($p < 0.001$ cluster corrected, left) whereas ITC$_{Cont6}$ was lower than ITC$_{Cont8}$ (left-temporal cluster, $p = 0.010$; right-frontal cluster $p = 0.005$, center). In the condition corresponding to 30°, instead ITC$_{Cont6}$ was greater than ITC$_{Cont4}$ ($p = 0.013$, right)

(B) In the condition corresponding to 15° resolution, a significant three-way interaction (experiment × ROI × periodicity) indicates different response profiles between the spatial (Figure 3B) and non-spatial experiment. In the non-spatial experiment, no significant differences between frequencies were identified in the left MTL ROI (top left), while in the right (bottom) MTL ITC$_{Cont6}$ was significantly lower than ITC$_{Cont8}$.

(C) In the condition corresponding to 30° resolution, a significant three-way interaction (experiment × ROI × periodicity) indicates different response profiles between the spatial (Figure 3C) and non-spatial experiment only in the left (top) and not in the right (bottom) hemisphere. This significant interaction was caused by ITC$_{Cont6}$ being greater than ITC$_{Cont4}$ in the left lateral occipital, in that no differences between experiments were found in the MTL. Gray dots indicate individual subjects. Error bars indicate standard error of the mean. Lines above data points indicate significance (n.s., not significant; *$p < 0.05$; **$p < 0.01$; ***$p < 0.001$).

See Table S1 for statistics of the pairwise comparisons.

Temporal structure of the FT design cannot explain the grid-like response

Temporal regularities in stimuli presentation constitute the most important feature of FT designs.[31] When multiple regularities are present (as in our case), their interaction can result in additional neural responses at frequencies corresponding to any sum of the originally tagged frequencies and their multiples (i.e., intermodulation[17,32]). Intermodulation of salient rhythms inherent to the previously presented FT design (e.g., presentation rate and "turn" of the clock-like presentation[33]) could potentially provide an alternative interpretation of the effects that were observed (Figure S8).

We thus conducted a control experiment to rule out the possibility that the grid-like response reported in the previous experiment was the by-product of other temporal regularities. Specifically, we designed another FT task having the same temporal regularities (i.e., the repeating sequences) but using non-spatially structured stimuli (i.e., letters). In the spatial experiment sequences were of different duration in the two angular resolutions, due to a difference in the number of trajectories. We replicated this feature using a different number of letters in the sequences (15°: 12 letters, from A to N; 30°: 6 letters, from A to F; see STAR Methods and Figure S9).

Data from 22 healthy participants who took part in this non-spatial experiment were analyzed following the same approach used in the spatial experiment (see STAR Methods). If the temporal structure of stimulus presentation and the interaction between multiple frequencies were the cause of the results in the spatial experiment, we should see a preference for the frequency that was previously tagged with 6-fold periodicity (i.e., 1.5 Hz in 15° resolution and 3 Hz in 30° resolution) in this non-spatial experiment as well. To test this hypothesis, we extracted the ITC of the frequencies that in the spatial experiment were tagged with spatial regularities (Figure 1B) and compared them at both sensor level and source level, both within and between experiments.

At sensor level, a two-sided cluster-permutation test (Figure 5A) in the condition that corresponded to the 15° angular resolution identified an occipito-temporal cluster in which ITC at the frequency corresponding to 6-fold spatial periodicity (ITC$_{Cont6}$) was greater than ITC at the frequency corresponding to 4-fold (ITC$_{Cont4}$) ($p < 0.001$ cluster corrected) and two clusters in which ITC at the frequency corresponding to 8-fold (ITC$_{Cont8}$) was higher than ITC$_{Cont6}$, one located in left temporal sensors ($p = 0.010$) and one in right frontal sensors ($p = 0.005$). In the condition

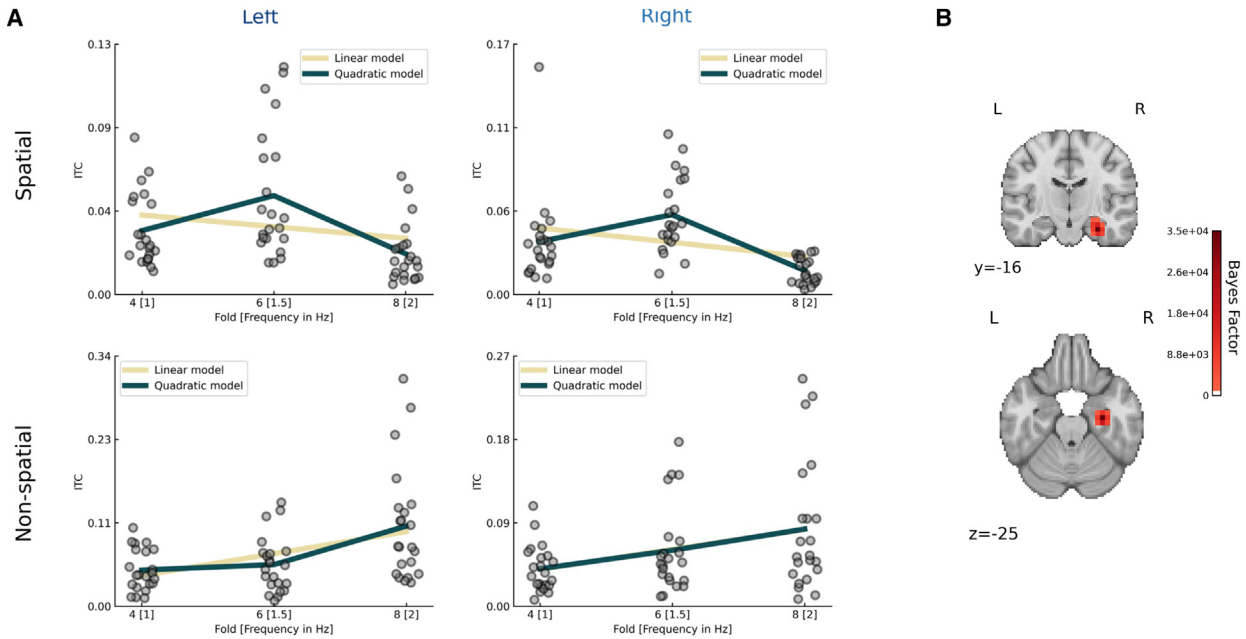

Figure 6. Bayesian model comparison identifies a quadratic trend in the spatial experiment and a linear trend in the non-spatial experiment

(A) In the spatial experiment (top), there was very strong evidence in favor of a quadratic model centered on ITC_6 as compared to a linear model in both the left (BF_{QL} = 150.05) and right (BF_{QL} = 2203.92) hemispheres. Conversely, in the non-spatial experiment, there was positive evidence for a linear model as compared to a quadratic model in the left hemisphere (BF_{LQ} = 8.07), while there was weak evidence for the linear model in the right hemisphere (BF_{LQ} = 2.04).

(B) Voxel-wise model comparison in the spatial experiment identified very strong evidence for the quadratic model as compared to the linear model in the MTL.

corresponding to 30°, we identified an occipito-temporal cluster in which ITC_{Cont6} was greater than ITC_{Cont4} ($p = 0.013$ cluster corrected). The condition corresponding to the 15° resolution showed clearly different results compared to the spatial experiment, with sensors in which ITC_{Cont8} was greater than ITC_{Cont6}. In the condition corresponding to the 30° resolution, with only one control periodicity, it was more difficult to characterize a grid-like response as compared to a more general response elicited by the temporal structure. Nevertheless, the topographies of the two experiments were different (Figure S10A), indicating a different neural origin of the effect. Moreover, we found a high correlation of the grid-like response (i.e., the difference between ITC_6 and ITC_4) between angular resolutions in the spatial experiment and not when correlating the corresponding frequencies of the non-spatial experiment (Figure S10B).

We then reconstructed the sources of the signal to further explore the effects elicited by the temporal structure and ensure that a 6-fold preference was not present in the MTL. Finally, we compared the ITC values in the ROIs between experiments using ANOVAs and Bayesian model comparison.

In the 15° condition (Figure 5B), a mixed ANOVA with experiment as between-subjects factor and ROI and periodicity as within-subjects factor identified a significant three-way interaction in both the left hemisphere ($F(2.73,114.58) = 39.43$, $p < 0.001$) and right hemisphere ($F(2.77, 116.27) = 22.93$, $p < 0.001$), indicating different patterns of ROI × periodicity interaction across the two experiments (spatial vs. non-spatial). Indeed, in the MTL the ITC_{Cont6} was never greater than both the control periodicities. Moreover, contrary to the spatial version of the experiment, the frequency preference showed similar trends in both the MTL and the control regions (see Figure 5B and Table S1 for post hoc pairwise comparison within each ROI). To directly compare ITC_6 with both control ITCs at the same time, we fitted (within each experiment) linear (L) and quadratic (Q) models to the group-level data and compared their goodness of fit with Bayes factor (BF[34]). In the MTL ROI (Figure 6A), we found very strong evidence[35] for the quadratic model centered on the 6-fold periodicity over the linear model in both the left hemisphere (BF_{QL} = 150.05) and right hemisphere (BF_{QL} = 2,203.92) in the spatial experiment. Conversely, in the non-spatial experiment, we found positive evidence for the linear model over the quadratic model in the left hemisphere (BF_{LQ} = 8.07) and weak evidence in the right hemisphere (BF_{LQ} = 2.04). This is confirmed at the cortical level, where the right MTL shows very strong evidence in favor of the quadratic model over the linear model in the spatial experiment (Figure 6B).

In the 30° resolution (Figure 5C), we found a significant three-way interaction (experiment × ROI × periodicity) in the left hemisphere ($F(1.3, 54.7) = 11.14$, $p < 0.001$) but not in the right hemisphere ($F(1.23, 51.84) = 2.56$, $p = 0.109$). Post hoc comparisons (Figure 5C and Table S1) revealed that a preference for the frequency that was previously tagged with 6-fold spatial periodicity was found in the bilateral MTL but, contrary to the spatial experiment, also in a control region, the left lateral occipital.

Taken together, these results demonstrated that the FT temporal structure generated different neural responses based on the task. The presentation of spatial sequences and their covert attentional tracking resulted in a grid-like response specific to

the MTL. The same temporal structure but no spatial allocation of attention instead produced different response profiles across the whole brain. In the 15° condition, we observed a linear increase of ITC with the frequency. In the 30° condition, it was more difficult to characterize the grid-like response as independent from other temporal regularities given the presence of a single control periodicity. Nevertheless, differences in both topographies and control regions make the MTL grid-like effect specific to the spatial experiment, suggesting differences in the mechanisms that gave rise to the observed response in the non-spatial experiment. In this respect, the left lateralization may be suggestive that lexical regularities (which have been shown to be detectable with FT[36,37]) were playing a role.

DISCUSSION

We demonstrated that a grid-like response, i.e., a preference for spatial trajectories aligned with a 6-fold periodicity as compared to control periodicities, was elicited in the human MTL by movements of attention. This effect arises in the absence of directly observable eye movements during the exploration of the environment, providing evidence that also in humans covert attention induces grid-like responses.

To this end, we used an eye tracker in combination with MEG FT. The proposed method relies on the periodic visual presentation of spatial trajectories. Crucially, unbeknownst to participants, these trajectories exhibited spatial regularities corresponding to the periodic firing of grid cells. This resulted in a grid-like response that was specific to the MTL, thus demonstrating the biological plausibility of the cellular-level signal that was picked up non-invasively with MEG. Moreover, in a control experiment, we provided evidence that the grid-like signal depended on covert movements of attention and not on the temporal structure of our task.

Covert attention elicited a grid-like signal in the human MTL

Previous literature had already demonstrated that overt visual exploration can result in a grid-like response in the MTL,[9–13] strengthening the relationship, in primates, between the neural mechanisms supporting spatial exploration through bodily and ocular movements.[7,8] Gaze location is often considered a proxy for spatial attention. However, attention can also be covertly moved in space independently of eye movements,[15] resulting in a similar grid-like response in non-human primates.[16] Here we demonstrated that a grid-like response was present also in humans while attention was covertly deployed to spatial locations.

By confirming findings from non-human primates, we provided comparable evidence across species for an attentional mechanism being able to give rise to grid-like responses. The current results allow for an interesting hypothesis regarding the general role of hippocampal cognitive maps in representing knowledge. Indeed, grid-like coding in the entorhinal cortex emerges also when people mentally explore relational links between non-spatial stimuli, such as visual objects,[38] odors,[39] social attributes,[40] or word meanings.[41] The attention-modulated activation of grid-like coding provides a suitable mechanism supporting the activation of the same hippocampal machinery during the navigation of conceptual spaces: where there is nothing to see and nowhere to move, but internal attention can be moved across the mental space.

In primates, attention and eye movements are tightly linked,[42–45] and it is possible that even spontaneous endogenous shifts of attention cannot be completely dissociated from gaze behavior, such as microsaccades.[46] Indeed, we found that similar trajectories induced similar biases in eye position, albeit very small. Across participants, however, the strength of this bias did not predict the grid-like effect, suggesting that it may not reflect attentional movements along the relevant spatial trajectories. However, if attentional movements cannot be completely dissociated from gaze behavior and if the navigation of conceptual spaces is mediated by attention, it could be possible that spontaneous eye movements would reflect the structure and navigation of abstract relational spaces. Future studies should investigate whether this is the case.

FT as a non-invasive tool to assess the grid-like response

A second purpose of the present study was to develop an alternative non-invasive method that allows detection of the grid-like response. The seminal paper by Doeller and colleagues[6] opened the possibility to study the proxy of a cellular response non-invasively, giving rise to numerous discoveries on the functioning of grid-like response in humans. While this method has been used successfully in both healthy participants and special populations,[47,48] it relied on participants' compliance to perform a task and undergo long training procedures. This greatly limited the possibility to investigate grid-like signals with populations that instead may have problems in performing cognitive tasks, such as patients, or may not be able to undergo long experiments, such as children.

We developed a method to detect a grid-like response based on FT that overcomes these limitations and can be used to further advance our understanding of grid-like responses in the human brain. FT in fact has been employed successfully in special populations.[49–51] Moreover, FT can be used to study high-level cognitive processes, such as attention[52,53] or understanding spatial relations.[54]

Taken together, our results indicate that the proposed method is a valid alternative to the now standard non-invasive analytical approaches to detect a grid-like signal, with the advantage of requiring less effort from the participants and thus being potentially useful in special populations.

Limitations of the study

In the present study we investigated the so-called grid-like response, a macro-scale proxy for the grid-cell response.[6] The relationship between grid-cell properties at the micro-scale and grid-like signal at the meso-scale and macro-scale, however, still have to be clarified.[55] Our FT paradigm, as well as other paradigms used in non-invasive neuroimaging (fMRI, MEG), may be able to capture such signal capitalizing on the coordinated activity of populations of conjunctive grid cells exhibiting similar orientations.[6,56] Nevertheless, it is also possible that

6-fold symmetry occurs independently at different levels of brain organization, with different and specific biological and behavioral relevance.[55] Future studies combining investigations at the micro-scale and meso-scale may shed light on the precise mechanism relating different levels of spatial representations.

Furthermore, studies recording field potentials will allow us to pinpoint the exact spatial origin of the signal we measured non-invasively with MEG. Mounting evidence demonstrates the ability of MEG to detect signals from deep brain structures such as the hippocampus.[57,58] Indeed, we observed a grid-like response specifically in the MTL and not in control regions, in line with other MEG studies focused on grid-like coding.[11,59] Nevertheless, distinguishing between subfields of the MTL may still be difficult, although simulation studies suggest it is possible.[60]

STAR★METHODS

Detailed methods are provided in the online version of this paper and include the following:

- KEY RESOURCES TABLE
- RESOURCE AVAILABILITY
  - Lead contact
  - Materials availability
  - Data and code availability
- EXPERIMENTAL MODEL AND STUDY PARTICIPANT DETAILS
- METHOD DETAILS
  - Spatial experiment design
  - Non-spatial experiment design
  - MEG and eye-tracker acquisition
  - MEG and eye-tracker preprocessing
  - Frequency analysis
  - Source reconstruction
- QUANTIFICATION AND STATISTICAL ANALYSIS
  - Behavioral analysis
  - Sensor-level cluster-permutation test
  - Source-level ROI analysis
  - Conjunction analysis
  - Source-level cluster-permutation test
  - Gaze- and dot-position correlation
  - Gaze distance to target dot
  - Spatial gaze modulation
  - Correlation between gaze and grid-like effects
  - Bayesian model comparison
  - Topographies' correlation

SUPPLEMENTAL INFORMATION

Supplemental information can be found online at https://doi.org/10.1016/j.celrep.2023.113209.

ACKNOWLEDGMENTS

This work was supported by the European Research Council ERC-StG NOAM awarded to R.B. (grant agreement no. 804422) and the Italian Ministry of Research MIUR FARE (protocol number R18WJMSNZF). We would like to thank Debottam Kundu, Francesco Romandini, and Mattia Silvestri for help in data collection.

AUTHOR CONTRIBUTIONS

Conceptualization, R.B.; methodology, G.G., L.V., Y.X., and R.B.; formal analysis, G.G. and L.V.; investigation, G.G.; writing – original draft, G.G.; writing – review & editing, G.G., L.V., Y.X., and R.B.; visualization, G.G.; supervision and funding acquisition, R.B.

DECLARATION OF INTERESTS

The authors declare no competing interests.

Received: February 8, 2023
Revised: August 25, 2023
Accepted: September 18, 2023

REFERENCES

1. Tolman, E.C. (1948). Cognitive maps in rats and men. Psychol. Rev. *55*, 189–208. https://doi.org/10.1037/h0061626.
2. Moser, E.I., Moser, M.-B., and McNaughton, B.L. (2017). Spatial representation in the hippocampal formation: a history. Nat. Neurosci. *20*, 1448–1464. https://doi.org/10.1038/nn.4653.
3. Hafting, T., Fyhn, M., Molden, S., Moser, M.-B., and Moser, E.I. (2005). Microstructure of a spatial map in the entorhinal cortex. Nature *436*, 801–806. https://doi.org/10.1038/nature03721.
4. Jacobs, J., Weidemann, C.T., Miller, J.F., Solway, A., Burke, J.F., Wei, X.-X., Suthana, N., Sperling, M.R., Sharan, A.D., Fried, I., and Kahana, M.J. (2013). Direct recordings of grid-like neuronal activity in human spatial navigation. Nat. Neurosci. *16*, 1188–1190. https://doi.org/10.1038/nn.3466.
5. Nadasdy, Z., Nguyen, T.P., Török, Á., Shen, J.Y., Briggs, D.E., Modur, P.N., and Buchanan, R.J. (2017). Context-dependent spatially periodic activity in the human entorhinal cortex. Proc. Natl. Acad. Sci. USA *114*, E3516–E3525. https://doi.org/10.1073/pnas.1701352114.
6. Doeller, C.F., Barry, C., and Burgess, N. (2010). Evidence for grid cells in a human memory network. Nature *463*, 657–661. https://doi.org/10.1038/nature08704.
7. Rolls, E.T., and Wirth, S. (2018). Spatial representations in the primate hippocampus, and their functions in memory and navigation. Prog. Neurobiol. *171*, 90–113. https://doi.org/10.1016/j.pneurobio.2018.09.004.
8. Nau, M., Julian, J.B., and Doeller, C.F. (2018). How the Brain's Navigation System Shapes Our Visual Experience. Trends Cognit. Sci. *22*, 810–825. https://doi.org/10.1016/j.tics.2018.06.008.
9. Killian, N.J., Jutras, M.J., and Buffalo, E.A. (2012). A map of visual space in the primate entorhinal cortex. Nature *491*, 761–764. https://doi.org/10.1038/nature11587.
10. Meister, M.L.R., and Buffalo, E.A. (2018). Neurons in Primate Entorhinal Cortex Represent Gaze Position in Multiple Spatial Reference Frames. J. Neurosci. *38*, 2430–2441. https://doi.org/10.1523/JNEUROSCI.2432-17.2018.
11. Staudigl, T., Leszczynski, M., Jacobs, J., Sheth, S.A., Schroeder, C.E., Jensen, O., and Doeller, C.F. (2018). Hexadirectional Modulation of High-Frequency Electrophysiological Activity in the Human Anterior Medial Temporal Lobe Maps Visual Space. Curr. Biol. *28*, 3325–3329.e4. https://doi.org/10.1016/j.cub.2018.09.035.
12. Julian, J.B., Keinath, A.T., Frazzetta, G., and Epstein, R.A. (2018). Human entorhinal cortex represents visual space using a boundary-anchored grid. Nat. Neurosci. *21*, 191–194. https://doi.org/10.1038/s41593-017-0049-1.

13. Nau, M., Navarro Schröder, T., Bellmund, J.L.S., and Doeller, C.F. (2018). Hexadirectional coding of visual space in human entorhinal cortex. Nat. Neurosci. *21*, 188–190. https://doi.org/10.1038/s41593-017-0050-8.

14. Bicanski, A., and Burgess, N. (2019). A Computational Model of Visual Recognition Memory via Grid Cells. Curr. Biol. *29*, 979–990.e4. https://doi.org/10.1016/j.cub.2019.01.077.

15. Posner, M.I. (1980). Orienting of attention. Q. J. Exp. Psychol. *32*, 3–25. https://doi.org/10.1080/00335558008248231.

16. Wilming, N., König, P., König, S., and Buffalo, E.A. (2018). Entorhinal cortex receptive fields are modulated by spatial attention, even without movement. Elife *7*, e31745. https://doi.org/10.7554/eLife.31745.

17. Norcia, A.M., Appelbaum, L.G., Ales, J.M., Cottereau, B.R., and Rossion, B. (2015). The steady-state visual evoked potential in vision research: A review. J. Vis. *15*, 4. https://doi.org/10.1167/15.6.4.

18. Tononi, G., Srinivasan, R., Russell, D.P., and Edelman, G.M. (1998). Investigating neural correlates of conscious perception by frequency-tagged neuromagnetic responses. Proc. Natl. Acad. Sci. USA *95*, 3198–3203. https://doi.org/10.1073/pnas.95.6.3198.

19. Stangl, M., Wolbers, T., and Shine, J.P. (2019). Population-Level Analysis of Human Grid Cell Activation. In Spatial Learning and Attention Guidance Neuromethods, S. Pollmann, ed. (Springer US), pp. 257–279. https://doi.org/10.1007/7657_2019_27.

20. Ding, N., and Simon, J.Z. (2013). Power and phase properties of oscillatory neural responses in the presence of background activity. J. Comput. Neurosci. *34*, 337–343. https://doi.org/10.1007/s10827-012-0424-6.

21. Ding, N., Melloni, L., Zhang, H., Tian, X., and Poeppel, D. (2016). Cortical tracking of hierarchical linguistic structures in connected speech. Nat. Neurosci. *19*, 158–164. https://doi.org/10.1038/nn.4186.

22. Henin, S., Turk-Browne, N.B., Friedman, D., Liu, A., Dugan, P., Flinker, A., Doyle, W., Devinsky, O., and Melloni, L. (2021). Learning hierarchical sequence representations across human cortex and hippocampus. Sci. Adv. *7*, eabc4530. https://doi.org/10.1126/sciadv.abc4530.

23. Maris, E., and Oostenveld, R. (2007). Nonparametric statistical testing of EEG- and MEG-data. J. Neurosci. Methods *164*, 177–190. https://doi.org/10.1016/j.jneumeth.2007.03.024.

24. Hari, R., and Salmelin, R. (2012). Magnetoencephalography: From SQUIDs to neuroscience. Neuroimage *61*, 386–396. https://doi.org/10.1016/j.neuroimage.2011.11.074.

25. Van Veen, B.D., Van Drongelen, W., Yuchtman, M., and Suzuki, A. (1997). Localization of brain electrical activity via linearly constrained minimum variance spatial filtering. IEEE Trans. Biomed. Eng. *44*, 867–880. https://doi.org/10.1109/10.623056.

26. Nichols, T., Brett, M., Andersson, J., Wager, T., and Poline, J.-B. (2005). Valid conjunction inference with the minimum statistic. Neuroimage *25*, 653–660. https://doi.org/10.1016/j.neuroimage.2004.12.005.

27. Wynn, J.S., Ryan, J.D., and Buchsbaum, B.R. (2020). Eye movements support behavioral pattern completion. Proc. Natl. Acad. Sci. USA *117*, 6246–6254. https://doi.org/10.1073/pnas.1917586117.

28. Lowet, E., Gomes, B., Srinivasan, K., Zhou, H., Schafer, R.J., and Desimone, R. (2018). Enhanced Neural Processing by Covert Attention only during Microsaccades Directed toward the Attended Stimulus. Neuron *99*, 207–214.e3. https://doi.org/10.1016/j.neuron.2018.05.041.

29. Liu, B., Nobre, A.C., and van Ede, F. (2022). Functional but not obligatory link between microsaccades and neural modulation by covert spatial attention. Nat. Commun. *13*, 3503. https://doi.org/10.1038/s41467-022-31217-3.

30. Yu, G., Herman, J.P., Katz, L.N., and Krauzlis, R.J. (2022). Microsaccades as a marker not a cause for attention-related modulation. Elife *11*, e74168. https://doi.org/10.7554/eLife.74168.

31. De Rosa, M., Ktori, M., Vidal, Y., Bottini, R., and Crepaldi, D. (2022). Frequency-based neural discrimination in fast periodic visual stimulation. Cortex *148*, 193–203. https://doi.org/10.1016/j.cortex.2022.01.005.

32. Gordon, N., Hohwy, J., Davidson, M.J., van Boxtel, J.J.A., and Tsuchiya, N. (2019). From intermodulation components to visual perception and cognition-a review. Neuroimage *199*, 480–494. https://doi.org/10.1016/j.neuroimage.2019.06.008.

33. Cracco, E., Lee, H., van Belle, G., Quenon, L., Haggard, P., Rossion, B., and Orgs, G. (2022). EEG Frequency Tagging Reveals the Integration of Form and Motion Cues into the Perception of Group Movement. Cerebr. Cortex *32*, 2843–2857, bhab385.. https://doi.org/10.1093/cercor/bhab385

34. Wagenmakers, E.-J. (2007). A practical solution to the pervasive problems ofp values. Psychon. Bull. Rev. *14*, 779–804. https://doi.org/10.3758/BF03194105.

35. Raftery, A.E. (1995). Bayesian Model Selection in Social Research. Socio. Methodol. *25*, 111–163. https://doi.org/10.2307/271063.

36. Lochy, A., Van Belle, G., and Rossion, B. (2015). A robust index of lexical representation in the left occipito-temporal cortex as evidenced by EEG responses to fast periodic visual stimulation. Neuropsychologia *66*, 18–31. https://doi.org/10.1016/j.neuropsychologia.2014.11.007.

37. Lochy, A., Jacques, C., Maillard, L., Colnat-Coulbois, S., Rossion, B., and Jonas, J. (2018). Selective visual representation of letters and words in the left ventral occipito-temporal cortex with intracerebral recordings. Proc. Natl. Acad. Sci. USA *115*, E7595–E7604. https://doi.org/10.1073/pnas.1718987115.

38. Constantinescu, A.O., OReilly, J.X., and Behrens, T.E.J. (2016). Organizing conceptual knowledge in humans with a gridlike code. Science *352*, 1464–1468. https://doi.org/10.1126/science.aaf0941.

39. Bao, X., Gjorgieva, E., Shanahan, L.K., Howard, J.D., Kahnt, T., and Gottfried, J.A. (2019). Grid-like Neural Representations Support Olfactory Navigation of a Two-Dimensional Odor Space. Neuron *102*, 1066–1075.e5. https://doi.org/10.1016/j.neuron.2019.03.034.

40. Park, S.A., Miller, D.S., and Boorman, E.D. (2021). Inferences on a multidimensional social hierarchy use a grid-like code. Nat. Neurosci. *24*, 1292–1301. https://doi.org/10.1038/s41593-021-00916-3.

41. Viganò, S., and Piazza, M. (2020). Distance and Direction Codes Underlie Navigation of a Novel Semantic Space in the Human Brain. J. Neurosci. *40*, 2727–2736. https://doi.org/10.1523/JNEUROSCI.1849-19.2020.

42. Rizzolatti, G., Riggio, L., Dascola, I., and Umiltá, C. (1987). Reorienting attention across the horizontal and vertical meridians: Evidence in favor of a premotor theory of attention. Neuropsychologia *25*, 31–40. https://doi.org/10.1016/0028-3932(87)90041-8.

43. Corbetta, M., Akbudak, E., Conturo, T.E., Snyder, A.Z., Ollinger, J.M., Drury, H.A., Linenweber, M.R., Petersen, S.E., Raichle, M.E., Van Essen, D.C., and Shulman, G.L. (1998). A Common Network of Functional Areas for Attention and Eye Movements. Neuron *21*, 761–773. https://doi.org/10.1016/S0896-6273(00)80593-0.

44. Smith, D.T., and Schenk, T. (2012). The Premotor theory of attention: Time to move on? Neuropsychologia *50*, 1104–1114. https://doi.org/10.1016/j.neuropsychologia.2012.01.025.

45. Awh, E., Armstrong, K.M., and Moore, T. (2006). Visual and oculomotor selection: links, causes and implications for spatial attention. Trends Cognit. Sci. *10*, 124–130. https://doi.org/10.1016/j.tics.2006.01.001.

46. Yuval-Greenberg, S., Merriam, E.P., and Heeger, D.J. (2014). Spontaneous Microsaccades Reflect Shifts in Covert Attention. J. Neurosci. *34*, 13693–13700. https://doi.org/10.1523/JNEUROSCI.0582-14.2014.

47. Kunz, L., Schröder, T.N., Lee, H., Montag, C., Lachmann, B., Sariyska, R., Reuter, M., Stirnberg, R., Stöcker, T., Messing-Floeter, P.C., et al. (2015). Reduced grid-cell-like representations in adults at genetic risk for Alzheimer's disease. Science *350*, 430–433. https://doi.org/10.1126/science.aac8128.

48. Bierbrauer, A., Kunz, L., Gomes, C.A., Luhmann, M., Deuker, L., Getzmann, S., Wascher, E., Gajewski, P.D., Hengstler, J.G., Fernandez-Alvarez, M., et al. (2020). Unmasking selective path integration deficits in

Alzheimer's disease risk carriers. Sci. Adv. *6*, eaba1394. https://doi.org/10.1126/sciadv.aba1394.

49. de Heering, A., and Rossion, B. (2015). Rapid categorization of natural face images in the infant right hemisphere. Elife *4*, e06564. https://doi.org/10.7554/eLife.06564.
50. Buiatti, M., Di Giorgio, E., Piazza, M., Polloni, C., Menna, G., Taddei, F., Baldo, E., and Vallortigara, G. (2019). Cortical route for facelike pattern processing in human newborns. Proc. Natl. Acad. Sci. USA *116*, 4625–4630. https://doi.org/10.1073/pnas.1812419116.
51. Vettori, S., Dzhelyova, M., Van der Donck, S., Jacques, C., Van Wesemael, T., Steyaert, J., Rossion, B., and Boets, B. (2020). Combined frequency-tagging EEG and eye tracking reveal reduced social bias in boys with autism spectrum disorder. Cortex *125*, 135–148. https://doi.org/10.1016/j.cortex.2019.12.013.
52. Müller, M.M., Malinowski, P., Gruber, T., and Hillyard, S.A. (2003). Sustained division of the attentional spotlight. Nature *424*, 309–312. https://doi.org/10.1038/nature01812.
53. Kim, Y.J., Grabowecky, M., Paller, K.A., Muthu, K., and Suzuki, S. (2007). Attention induces synchronization-based response gain in steady-state visual evoked potentials. Nat. Neurosci. *10*, 117–125. https://doi.org/10.1038/nn1821.
54. Adibpour, P., Hochmann, J.-R., and Papeo, L. (2021). Spatial Relations Trigger Visual Binding of People. J. Cognit. Neurosci. *33*, 1343–1353. https://doi.org/10.1162/jocn_a_01724.
55. Kunz, L., Maidenbaum, S., Chen, D., Wang, L., Jacobs, J., and Axmacher, N. (2019). Mesoscopic Neural Representations in Spatial Navigation. Trends Cognit. Sci. *23*, 615–630. https://doi.org/10.1016/j.tics.2019.04.011.
56. Stensola, H., Stensola, T., Solstad, T., Frøland, K., Moser, M.-B., and Moser, E.I. (2012). The entorhinal grid map is discretized. Nature *492*, 72–78. https://doi.org/10.1038/nature11649.
57. Ruzich, E., Crespo-García, M., Dalal, S.S., and Schneiderman, J.F. (2019). Characterizing hippocampal dynamics with MEG: A systematic review and evidence-based guidelines. Hum. Brain Mapp. *40*, 1353–1375. https://doi.org/10.1002/hbm.24445.
58. Pu, Y., Cheyne, D.O., Cornwell, B.R., and Johnson, B.W. (2018). Non-invasive Investigation of Human Hippocampal Rhythms Using Magnetoencephalography: A Review. Front. Neurosci. *12*, 273. https://doi.org/10.3389/fnins.2018.00273.
59. Convertino, L., Bush, D., Zheng, F., Adams, R.A., and Burgess, N. (2023). Reduced grid-like theta modulation in schizophrenia. Brain *146*, 2191–2198, awac416.. https://doi.org/10.1093/brain/awac416
60. Stephen, J., Ranken, D., Aine, C., Weisend, M., and Shih, J. (2005). Differentiability of simulated MEG hippocampal, medial temporal and neocortical temporal epileptic spike activity, pp. 388–401.
61. Gramfort, A., Luessi, M., Larson, E., Engemann, D.A., Strohmeier, D., Brodbeck, C., Goj, R., Jas, M., Brooks, T., Parkkonen, L., and Hämäläinen, M. (2013). MEG and EEG data analysis with MNE-Python. Front. Neurosci. *7*, 267.
62. Harris, C.R., Millman, K.J., van der Walt, S.J., Gommers, R., Virtanen, P., Cournapeau, D., Wieser, E., Taylor, J., Berg, S., Smith, N.J., et al. (2020). Array programming with NumPy. Nature *585*, 357–362. https://doi.org/10.1038/s41586-020-2649-2.
63. Hunter, J.D. (2007). Matplotlib: A 2D Graphics Environment. Comput. Sci. Eng. *9*, 90–95. https://doi.org/10.1109/MCSE.2007.55.
64. Virtanen, P., Gommers, R., Oliphant, T.E., Haberland, M., Reddy, T., Cournapeau, D., Burovski, E., Peterson, P., Weckesser, W., Bright, J., et al. (2020). SciPy 1.0: fundamental algorithms for scientific computing in Python. Nat. Methods *17*, 261–272. https://doi.org/10.1038/s41592-019-0686-2.
65. McKinney, W. (2010). Data Structures for Statistical Computing in Python, pp. 56–61. https://doi.org/10.25080/Majora-92bf1922-00a.
66. Seabold, S., and Perktold, J. (2010). Statsmodels: Econometric and Statistical Modeling with Python, pp. 92–96. https://doi.org/10.25080/Majora-92bf1922-011.
67. Brainard, D.H. (1997). The Psychophysics Toolbox. Spatial Vis. *10*, 433–436. https://doi.org/10.1163/156856897X00357.
68. Taulu, S., and Simola, J. (2006). Spatiotemporal signal space separation method for rejecting nearby interference in MEG measurements. Phys. Med. Biol. *51*, 1759–1768. https://doi.org/10.1088/0031-9155/51/7/008.
69. Waskom, M. (2021). seaborn: statistical data visualization. J. Open Source Softw. *6*, 3021. https://doi.org/10.21105/joss.03021.
70. Benjamin, L., Dehaene-Lambertz, G., and Fló, A. (2021). Remarks on the analysis of steady-state responses: Spurious artifacts introduced by overlapping epochs. Cortex, S0010945221002215. https://doi.org/10.1016/j.cortex.2021.05.023.
71. Oostenveld, R., Fries, P., Maris, E., and Schoffelen, J.-M. (2011). FieldTrip: Open Source Software for Advanced Analysis of MEG, EEG, and Invasive Electrophysiological Data. Comput. Intell. Neurosci. *2011*, e156869. https://doi.org/10.1155/2011/156869.
72. Fischl, B. (2012). Neuroimage *62*, 774–781. https://doi.org/10.1016/j.neuroimage.2012.01.021.
73. Vinding, M.C., and Oostenveld, R. (2022). Sharing individualised template MRI data for MEG source reconstruction: A solution for open data while keeping subject confidentiality. Neuroimage *254*, 119165. https://doi.org/10.1016/j.neuroimage.2022.119165.
74. Westner, B.U., Dalal, S.S., Gramfort, A., Litvak, V., Mosher, J.C., Oostenveld, R., and Schoffelen, J.-M. (2022). A unified view on beamformers for M/EEG source reconstruction. Neuroimage *246*, 118789. https://doi.org/10.1016/j.neuroimage.2021.118789.
75. Desikan, R.S., Ségonne, F., Fischl, B., Quinn, B.T., Dickerson, B.C., Blacker, D., Buckner, R.L., Dale, A.M., Maguire, R.P., Hyman, B.T., et al. (2006). An automated labeling system for subdividing the human cerebral cortex on MRI scans into gyral based regions of interest. Neuroimage *31*, 968–980. https://doi.org/10.1016/j.neuroimage.2006.01.021.
76. Fischl, B., Salat, D.H., Busa, E., Albert, M., Dieterich, M., Haselgrove, C., van der Kouwe, A., Killiany, R., Kennedy, D., Klaveness, S., et al. (2002). Whole Brain Segmentation: Automated Labeling of Neuroanatomical Structures in the Human Brain. Neuron *33*, 341–355. https://doi.org/10.1016/S0896-6273(02)00569-X.
77. R. (2022). A Language and Environment for Statistical Computing.
78. Kuiper, N.H. (1960). Tests concerning random points on a circle. Indag. Math. Proc. *63*, 38–47. https://doi.org/10.1016/S1385-7258(60)50006-0.

STAR★METHODS

KEY RESOURCES TABLE

REAGENT or RESOURCE	SOURCE	IDENTIFIER
Software and algorithms		
Python 3.9	Python Software Foundation	RRID:SCR_008394
MNE-python	Gramfort et al.[61]	RRID:SCR_005972
Numpy	Harris et al.[62]	RRID:SCR_008633
Matplotlib	Hunter et al.[63]	RRID:SCR_008624
Scipy	Virtanen et al.[64]	RRID:
Nilearn	https://nilearn.github.io/stable/index.html	RRID:SCR_001362
Pandas	McKinney et al.[65]	RRID:SCR_018214
Seaborn	Waskom [62]	RRID:SCR_018132
Statsmodel	Seabold et al.[66]	RRID:SCR_016074
MATLAB 2012b	Mathworks	RRID:SCR_001622
Psychtoolbox	Brainard [67]	RRID:SCR_002881
R	R Core Team, 2022	RRID:SCR_001905
Custom code	This paper	DOI: 10.17605/OSF.IO/TV2CU

RESOURCE AVAILABILITY

Lead contact

Further information and requests should be directed to and will be fulfilled by the lead contact Roberto Bottini, roberto.bottini@unitn.it.

Materials availability

This study did not generate new unique reagents.

Data and code availability

- Data reported in this paper will be shared by the lead contact upon request.
- All original code has been deposited at DOI 10.17605/OSF.IO/TV2CU
- Any additional information required to reanalyze the data reported in this paper is available from the lead contact upon request.

EXPERIMENTAL MODEL AND STUDY PARTICIPANT DETAILS

Twenty-four participants (12 male, age M = 25,88 years; SD = 4,84) were recruited to participate in the spatial experiment that consisted in two magnetoencephalography (MEG) sessions, conducted in different days (maximum eight days apart). One participant did not show up for the second session and was excluded from the analysis. Another sample of twenty-four participants (9 male, age M = 23,91 years; SD = 3,51) were recruited to participate in the non-spatial experiment.

All had normal or corrected to normal vision and no history of neurological disorders. Prior to each session they gave written informed consent to participate in the experiment. All procedures were approved by the ethical committee of the University of Trento.

METHOD DETAILS

Spatial experiment design

The experiment consisted in the visual presentation of spatial stimuli (trajectories). These were defined dividing a circle in 24 and 12 equidistant points, resulting in two angular resolutions (15° and 30°) that were presented in different trials. These points were rotated 10° clockwise to avoid trajectories to appear along the cardinal axes. Each trajectory connected two opposite points (i.e., 180° apart) in the circle.

In separate recording sessions these trajectories were presented to the same participants either as a sequence of dots, moving from one end to the other of the circle, or as static lines, covering the whole trajectory at once. The order of the sessions was

counterbalanced across participants. Note that static lines lack directionality, effectively reducing the number of trajectories to half. That is, a trajectory starting at 20° and ending at 200° occupied the same portion of space as a trajectory starting at 200° and ending at 20°. In the dots session half of the trajectories were presented as starting from the opposite side of the circle, effectively making opposite trajectories indistinguishable between each other. The total number of trajectories is thus 12 in the 15° resolution and 6 in the 30° resolution.

Stimuli were generated using MATLAB (version 2012b, The Mathworks, Natick, MA, USA) and presentation was controlled using PsychToolbox.[67]

A new trajectory was presented every 0.166 s (6 Hz) using a typical frequency-tagging (FT) approach (Figure 1). In the "lines" session, a new line appeared at the presentation rate of 6 Hz crossing the circle from one end to the other with a break around the fixation window. In the "dots" session individual trajectories were presented at 6 Hz but they were formed by 20 dots, appearing in successive positions along the trajectory at the rate of 0.0083 s (corresponding to the 120 Hz refresh rate of the screen) and covering the whole trajectory before the appearance of the next one. Of these 20 dots, the 4 central dots were excluded to avoid presenting them within the fixation window. In each trial were presented 264 trajectories, for a total duration of 44 s. These appeared sequentially, in a clock-like fashion (e.g., 20°, 50°, 80°, 110° etc … in the 30° resolution, Figure 1A), with clockwise/counter-clockwise direction balanced across participants. Crucially, the periodic presentation of regularly spaced trajectories allowed to embed multiple spatial periodicities in the trajectories' sequence, each appearing at fixed and distinct temporal intervals such that each spatial periodicity "tags" a unique frequency (Figure 1B). Specifically, at 15° resolution, trajectories separated by 60° (6-fold) appear every 0.666 s (1.5 Hz), trajectories separated by 90° (4-fold) every 1 s (1 Hz) and trajectories separated by 45° (8-fold) every 0.5 s (2 Hz). At 30° instead, trajectories separated by 60° appear every 0.333 s (3 Hz) while trajectories separated by 90° appear every 0.5 s (2 Hz). Note that 6- and 4-fold occur in both spatial resolutions, but tagging different frequencies in each. This enables an estimation of their neural tracking that is not tied to a specific chosen frequency as well as direct comparison between responses in the two spatial resolutions.

Multiple sequences with the same trajectories' order were presented in a trial to allow the emergence of a frequency-tagged response to the different spatial periodicities. Specifically, individual sequences lasted 2 s (15°) and 1 s (30°), with each sequence containing one instance of each trajectory. With the clock-like presentation one sequence corresponds to half-turn of the clock. The starting trajectory of the sequence was randomized across trials such that each trajectory was used as a start twice (15°) or four times (30°) over the experiment.

Participants were instructed to fixate in the center of the screen while paying attention to the trajectories that were shown in the periphery. To avoid following saccades, we defined a fixation window of 4.5° of visual angle[16] in which no visual stimulus was presented, except for a fixation dot that remained on the screen center for the whole trial duration. This fixation window size was used also to restrict participants gaze behavior: at the end of each trial, a warning message appeared on the screen if the participant's gaze was outside the fixation window for more than 20% of the trial time (8.4 s).

To ensure participants were covertly tracking the trajectories, we asked them to perform a location memory task (Fig., 1D). Two red target dots appeared at random position along a trajectory for 0.025 s. The timing of their appearance was randomized but constrained between 19 and 33 s for the first dot and between 37 and 39 s for the second dot. This timing was chosen to ensure participants were focused until the end of the FT presentation. Participants were instructed to remember the exact position of these two red target dots for future recall. At the end of each trial two red test dots appeared in three possible configurations, each with equal probability: i) test dots occupy the same spatial positions as target dots; ii) only one test dot does not occupy the same position of the target dots; iii) there was no overlap between test and target dots. Participants had to respond via button-press with the right index finger to indicate same position and with the right middle finger to indicate different position, irrespective of the number of dots being in a different position. The probability of these occurrences was 50%.

The experiment was divided in six blocks of eight trials each, for a total of 48 trials, 24 in each angular resolution. In each block there were four consecutive trials of the same angular resolution, and the resolution presented as first was randomized and balanced across blocks.

The timing of the presentations was controlled by the computer. A 15 s break was included after every trial, while 30 s were allowed after 4 consecutive trials. After each break, a 3 s countdown informed participants that a new trial was about to start. The trial then only started after participants had fixated for at least 500 ms within a 2° visual angle fixation window centered on the fixation dot. After each block participants were allowed a longer, self-timed, break of about 2 min.

Non-spatial experiment design

With this control experiment we wanted to test the hypothesis that temporal regularities inherent to the FT design can generate a periodic neural response that is comparable to the grid-like signal measured in the spatial experiment. Temporal regularities are defined here by the number of stimuli presented in the sequence and the individual sequences' duration, which varied between the angular resolutions of the spatial experiment. We thus reproduced these features using stimuli without spatial structure. Specifically, we reproduced the temporal structure of the 15° resolution by creating a sequence of 12 letters (A to N). Similarly, the 30° resolution was reproduced by creating a sequence of 6 letters (A to F).

Individual letters were visually presented every 0.166 s (6 Hz) with contrast modulation.[36,37] Other potentially salient temporal regularities that may be tagged by this FT design include the sequence duration. Sequences corresponding to the 15° resolution lasted

2 s (0.5 Hz) while sequences corresponding to 30° resolution lasted 1 s (1 Hz). Frequencies of interest in the spatial experiment are not tagged with spatial regularities anymore. Any effect observed at these frequencies cannot be ascribed to spatial regularities but should be interpreted as arising from the intermodulation of the presentation rate and other potentially salient rhythms such as the sequence rate.

Participants were instructed to fixate in the center of the screen while paying attention to the letters' sequences. Moreover, to keep them engaged, twice during a trial and with the same time constraints as in the spatial experiment the fixation dot turned red for 0.025 s, a change that the participants were instructed to promptly detect (max 3 s) via right index finger button press.

MEG and eye-tracker acquisition

MEG data were acquired at the Center for Mind/Brain Sciences of the University of Trento with an Elekta Neuromag 306 MEG system (Elekta, Helsinki, Finland), composed of 102 magnetometers and 204 planar gradiometers, placed in a magnetically shielded room (AK3B, Vakuumschmelze, Hanau, Germany). The head-shape of the participants was digitized (Fastrak Polhemus, Inc., Colchester, VA, USA) prior to acquisition in each session, along with fiducial points (nasion, left and right periauricular) and five head position indicator (HPI) coils, three placed on the forehead and one behind each ear. Both fiducials and HPIs were digitized twice to ensure precision (<2 mm difference).

Before entering the MEG, participants performed a short practice block (4 trials, 2 of each angular resolution) to familiarize with the FT design and the task. They received written instructions before the practice and feedback on their performance after each trial.

Participants sat upright in the MEG chair with their head as close as possible to the dewar. The eye-tracker (Eyelink 1000 Plus, SR Research Ltd., Ottawa, Canada) was positioned to ensure optimal recording of both eyes. A nine-point calibration procedure was carried out before each block.

Continuous MEG data were recorded at 1000 Hz with hardware bandpass filters in the range 0.1–330 Hz. Along with MEG, we also recorded the time series of a photodiode that tracked the colour-change of a small square on the top-left corner of the screen (not visible to the participants). This color-change was coded as indicating the start of a trial and was used in the analysis to correct for potential delays in the stimuli presentation. Eye-tracker was recorded separately for each trial at a sampling rate of 1000 Hz. Stimuli were projected on a translucent whiteboard, positioned 1 m in front of the participant, using a ProPixx projector (Vpixx Technologies, Canada) at a 120 Hz refresh rate. Responses were collected using a MEG compatible button response box (Vpixx Technologies, Canada).

After each session a 5 min empty-room measurement was recorded to be used for noise modeling in the source reconstruction procedure.

Four blocks from different participants had technical issues and were not included in the final analysis.

MEG and eye-tracker preprocessing

Raw task data and empty-room MEG time series were visually inspected to identify sensors with jumps and noise throughout the recording session. Artifactual sensors (M = 7.59, SD = 6.75) were excluded and interpolated through MaxFilter (temporal signal suppression[68]). Raw task data was subsequently realigned to the recording block that minimized the Euclidean distance across blocks, separately for each session.

Further processing and visualization were conducted in python using MNE-python[61] as well as common scientific python packages.[62–66,69]

After application of MaxFilter, continuous raw data were filtered (High pass: 0.1 Hz, Low-pass: 40 Hz) and segmented into 44 s–long trials, starting from the onset of the first trajectory. Trial onset was corrected for potential delays using a photodiode: we replaced the MEG-recorded trigger with the actual time indicated by the change in the photodiode time series, thus setting the trial onset to the actual presentation of the first trajectory on the screen as viewed by the participant.

Hence, for each trial we quantified fixation behavior by computing the percentage of time the right eye position was within the 4.5° fixation window. Trials in which this metric was below 80% of the trial time (35.6 s) were excluded from further analysis (percentage of rejected trials: spatial experiment: dots session: 5.7%; lines session: 5.1%; non-spatial experiment: 7.69%). In the non-spatial experiment one participant was excluded at this stage due to the low number of trials left after exclusion (33%).

In a control analysis (dots and lines session only, Fig.S4), we removed trials with fixation time below 95% (41.8 s). This led to the exclusion of one participant for which the total number of trials left was below 33%, leaving 21 participants for this control analysis.

To ensure consistent timing across trials in the appearance of the spatial periodicities, trials were realigned to the first presentation of the 350° trajectory, reducing their length to 40 s and 42 s in the 15° and 30° resolution, respectively.

To increase the signal-to-noise ratio,[70] trials' time series were further divided in shorter, non-overlapping segments of 8 s and 6 s, resulting in 5 and 7 segments per trial in the 15° and 30° resolution, respectively. Segment duration was chosen for multiple reasons: i) It allows an integer number of repetitions of each individual sequence (4 and 6); ii) each segment contains an integer number, as well as a high number, of cycles of the frequencies of interest and enables as a high frequency resolution (0.125 Hz and 0.167 Hz), resulting in output frequencies that match the tagged frequencies. Segmented data underwent a semi-automatic artifact rejection procedure in which both variance and kurtosis were computed over time for each channel, akin to the visual artifact rejection procedure implemented in the Fieldtrip package,[71] and subsequently averaged across channels to obtain a metric per segment. Segments above two standard deviations in each individual metric were visually inspected for the presence of artifacts (e.g., remaining channel jumps,

muscle artifacts, blinks). If visual inspection confirmed the presence of an artifact, the segment was marked as bad and excluded from further analyses. This procedure led to the exclusion of an additional 0.68% of segments in the dots session of the spatial experiment and 1.04% of segments in the lines session, while 0.83% of segments were excluded in the non-spatial experiment.

Frequency analysis

Artifact-free segments were subjected to a fast-Fourier transform (FFT) separately for each channel (at sensor-level) or voxel (at source level). From the complex representation of each segments' time series in the frequency domain we computed the inter-trial coherence (ITC) as follows:

$$ITC = \left(\frac{1}{N}\sum_{n=1}^{N} cos\ \theta_n\right)^2 + \left(\frac{1}{N}\sum_{n=1}^{N} sin\ \theta_n\right)^2$$

where θ is the phase of the individual segment (n) as obtained from the FFT.[20–22]

This metric quantifies the synchronization of the neural response across segments and ranges from 0 to 1, where 1 indicates perfect synchronization. We then isolated the ITC at the single individual frequencies "tagged" with the spatial periodicities (see "Spatial experiment design" and Figure 1B), given the narrowband response afforded by the FT method. For comparison, the same frequencies were selected in the non-spatial experiment. However, these frequencies bore no spatial meaning, as in this control experiment they were not tagged with spatial regularities.

Source reconstruction

Structural T1-weighted images were acquired at the Center for Mind/Brain Sciences of the University of Trento in a 3T Siemens Prisma scanner (Siemens, Erlangen, Germany) with a Multi-Echo MPRAGE (MEMPRAGE) sequence with the following parameters: FoV = 256mm; Voxel Size = 1 × 1 × 1 mm3; TR = 2530 ms; TE1 = 1.69ms; TE2 = 3.55ms; TE3 = 5.41ms; TE4 = 7.27ms and a flip angle of 7°. Two participants of the spatial experiment did not perform the MRI session.

Anatomical images were segmented using Freesurfer 7[72] to obtain subject-specific anatomical parcellations.

Coregistration of the digitized head position and the reconstructed structural surfaces was performed separately for each session. First the three fiducial points were matched, followed by an iterative closest-point match algorithm that minimizes the distance between the digitized head shape and the skin surface. For the two participants without MRI this procedure consisted in warping the Freesurfer template to match their digitized head shape and derive a subject-specific template. As recently demonstrated, using a template produces highly similar results than using the subject-specific T1 image.[73]

A single shell boundary-element method model was created to define a volume source space by filling the inner skull surface with equidistant (5 mm) voxels.

Inverse solution was based on linearly-constrained minimum variant (LCMV) beamformer.[25] A beamformer approach was chosen given its better resolution in estimating subcortical activity.[57,58] A time domain solution was preferred to be able to reconstruct multiple frequencies at source level using a single spatial filter, such that the observed differences cannot be ascribed to differences in the inversion algorithm. Artifact-free segments, including data of both magnetometers and gradiometers, were used for source reconstruction. From these we estimated the empirical data covariance (separately for the 15° and 30° resolutions) while subject specific empty-room recordings were used to model noise and account for the different contributions of the two sensor types. Both data and noise covariance matrices were regularized with 5% of the sensors' power and their rank was reduced to the residual degrees of freedom after application of MaxFilter.[74] Inversion kernel dimensionality was reduced by one dimension, as suggested for MEG data with single-shell headmodel. Dimensionality of the inversion kernel was further reduced by retaining (through SVD) the dipole orientation that maximized power, resulting in a scalar beamformer. No depth weighting was applied. Beamformer weights were normalized using the 'unit-noise-gain-invariant' option. The FFT and then ITC were computed at each voxel from the reconstructed time series as detailed in the frequency analysis section.

In a control analysis we replicated the source reconstruction procedure detailed above but using only magnetometers data (Figure S5).

QUANTIFICATION AND STATISTICAL ANALYSIS

Behavioral analysis

Accuracy (percentage of correct responses) was computed separately for each session and each angular resolution. We used a dependent samples t test to compare these metrics across angular resolutions, separately for each session. One participant of the spatial experiment was excluded from further analysis due to performance being two standard deviation below the group mean in both session. Similarly, one participant in the non-spatial experiment was excluded based on the same criterion.

Sensor-level cluster-permutation test

A two-sided cluster-based permutation test[23] was used to compare the ITC at the frequency corresponding to the 6-fold spatial periodicity ($ITC_{6:}$ 1.5 Hz in the 15° resolution, 3 Hz in the 30° resolution) to the ITC of the control spatial periodicities (15° resolution:

ITC_8 2 Hz, ITC_4 1 Hz; 30° resolution: ITC_4 2 Hz), separately for each angular resolution and each control periodicity. For this analysis we considered only magnetometers, given their higher sensitivity to deep brain structures as compared to planar gradiometers.[24]

In brief, a one-sample t test is performed at each channel on the difference between conditions (i.e., spatial periodicities). The channels that survived an uncorrected threshold of $p < 0.05$ are retained to form spatial clusters based on a predefined adjacency matrix with ~6 neighbors per channel. This procedure was repeated 10000 times, each time shuffling the condition labels and retaining the highest cluster statistic (t-score). A p value corrected for multiple comparisons is obtained by comparing the cluster statistic observed from the actual contrast with the distribution of permuted cluster statistics.

The same analysis was applied to the non-spatial experiment data, comparing the frequencies that in the spatial experiment were tagged with spatial regularities.

Source-level ROI analysis

Source level analysis focused on subject-specific anatomical regions of interest (ROIs) obtained from the Freesurfer parcellation. Specifically, we created an MTL ROI encompassing the entorhinal and parahippocampal cortex, from the Desikan-Killiany atlas,[75] and the hippocampus, obtained from Freesurfer's own subcortical parcellation.[76] We included control ROIs from the Desikan-Killany atlas to confirm the specificity of the effect in the medial temporal lobe. As control ROIs we used the lateral occipital, to test for an effect in visual cortex given the visual nature of the task. The precentral ROI was chosen as a region that was supposed to be distant from the effects of interest.

Subject-specific, average ITC values within each ROI were entered into series of analysis of variance (ANOVA) in R.[77] First, a two-way repeated measures ANOVA with factors session (dots, lines) x periodicity (15° resolution: 4-, 6-, 8-fold; 30° resolution: 4-, 6-fold) was aimed at investigating differences in the neural tracking in the MTL ROI between the dots and lines sessions. This analysis was repeated for each hemisphere and each angular resolution. Results showed no statistically significant session × periodicity interaction, suggesting that a similar response profile could be observed across sessions. All subsequent analyses will therefore consider the average across session as input.

A two-way repeated measures ANOVA with factors ROI (MTL, lateral occipital, precentral) x periodicity (15° resolution: 4-, 6-, 8-fold; 30° resolution: 4-, 6-fold) investigated differences across ROIs in the neural tracking of the spatial periodicities. Planned paired t-tests were conducted to evaluate whether ITC_6 was greater than ITC of the control periodicities in each ROI.

Last, we compared the spatial experiment to the non-spatial experiment. We conducted a three-way mixed ANOVA with experiment (spatial, non-spatial) as between-subjects factor and ROI (MTL, lateral occipital, precentral) and periodicity (15° resolution: 4-, 6-, 8-fold; 30° resolution: 4-, 6-fold) as within-subject factors.

Greenhouse-Geisser correction was applied to the degrees of freedom in case sphericity assumption was violated.

Conjunction analysis

ROI analysis is biased by *a-priori* selection of a limited number of regions, effectively neglecting contributions from other parts of the brain. To assess whether this constraint hinders the interpretation of our findings we additionally computed a whole-brain conjunction analysis.[25] This consists in computing the individual contrasts between ITC_6 and ITC of the control periodicities, separately for each cortical voxel and for each angular resolution. The resulting t-maps are then combined by retaining, for each voxel, the minimum t-value across all contrasts and angular resolutions. Resulting t-maps are plotted at an uncorrected threshold of $p < 0.005$.

This analysis highlights the commonalities between contrasts, thus providing the best visualization of the spatial specificity of the grid-like effect, that is independent of the specific tagged frequencies and angular resolutions.

Source-level cluster-permutation test

We also performed a cluster-permutation test[23] at the cortical level. In the 15° resolution we contrasted ITC_6 to the averaged ITC_4 and ITC_8. In the 30° resolution we contrasted ITC_6 to ITC_4. The procedure was the same as the one described in the paragraph "Sensor-level cluster-permutation test", except that in these analyses clusters were formed by voxels in volume source space instead of sensors.

Gaze- and dot-position correlation

We investigated whether the eyes were following the dots by replicating the control analyses conducted by Wilming and colleagues.[16] First, the eye tracker data were downsampled to 120 Hz to match the screen refresh rate, at which dots were presented. Then, for each trial, we computed the Euclidean distance between the eye position and the center of the screen at each time point. Similarly, the Euclidean distance was computed between the dot position and the center of the screen at each time point. The time points when a blink was detected were excluded from both vectors before computing the Euclidean distance. We then correlated the resulting distance vectors. A positive correlation would indicate that the eyes were following the dot. The resulting r values were fisher transformed and entered in a one-sample t test against zero, separately for 15° and 30° resolution, and in a dependent samples t test to compare between the angular resolutions. This analysis was conducted only for the dots session, for which we could precisely estimate one spatial location of the stimuli per time point.

Gaze distance to target dot

We investigated whether the presentation of target dots induced a shift in gaze location toward the target dot location. Separately for each target dot presentation, we computed the Euclidean distance between the eye position and the target dot position. We then selected two time windows of interest: −0.05 to 0 s and 0.05 to 0.1 s relative to target dot onset (see Ref 29 for a similar time window definition), i.e., "before" and "after" the target dot onset. If the eye had followed the dot, its distance in the "after" time window would have been smaller as compared to the "before" time window. We thus compared the average gaze distance between time windows using a paired samples t test, separately for each session and angular resolution.

Spatial gaze modulation

We implemented further control analyses on the eye-tracker data to investigate gaze behavior in both the dots and the lines session.

We segmented the trial time series according to the presentation of the trajectories and concatenated the time windows corresponding to the same trajectory (separately for each session and angular resolution), excluding all time points in which gaze was outside the fixation window.

The aggregated time series were transformed into heatmaps using Gaussian kernel density estimate,[27] as implemented in scipy with default parameters.

This process was repeated for each individual trajectory resulting in 12 and 6 heatmaps for 15° and 30° angular resolution, respectively (Figure 4B for an example of 30° resolution heatmaps). Each pair of heatmap (separately for each angular resolution) was then correlated using Pearson correlation, resulting in 66 correlation values in 15° resolution and 15 values in 30° resolution. The average (within-subject) pairwise correlation is reported in Figure 4C and in the main text. We then computed the angular difference between the pairs of trajectories. This difference was normalized between 0° and 90° to account for the circularity of the angular measure. The vector of pairwise correlations between the heatmaps was then correlated with the vector of corresponding angular differences. The resulting correlation values were fisher transformed and entered in a one sample t test against zero.

Similarly, the aggregated time series of gaze location were used to compute the gaze angle with respect to the screen center for each trajectory. Gaze-angles distributions (12 in 15°, 6 in 30°; Figure S7A) of each trajectories pair (66 in 15°, 15 in 30°) were compared using Kuiper's test,[78] whose test statistic "V" indexes the difference between pairs of circular distributions, with larger values indicating larger differences. The average (within-subject) test statistic is reported in Figure S7B. The normalized angular difference was correlated with the corresponding V score. The resulting r scores were fisher transformed and tested at the group-level against the null hypothesis of no correlation.

Correlation between gaze and grid-like effects

We further investigated whether gaze behavior was playing a role in the generation of the grid-like response. To do this we computed correlation between the grid-like measure and the measure of trajectory-based gaze similarity as obtained in the previous analyses. As grid-like measure we used the slope of a quadratic model fitted on the ITC response in MTL of each subject in the 15° resolution (see "*Bayesian model comparison*" for a similar analysis on the group-level data). Similarly, in the 30° resolution we used the slope of a linear model. As trajectory-based gaze similarity measure we used the slope of the correlation between trajectories' angular difference and the corresponding similarity measure (r for heatmaps, v for gaze-angles distributions). We computed Pearson's correlation between these measures to investigate whether participants that showed a higher grid-like effect were also the ones whose gaze was more influenced by the presentation of the trajectories.

Bayesian model comparison

To directly compare the ITC_6 with both control ITCs at the same time, we fitted linear and quadratic models to the group-level ROI data at 15° resolution. For both linear and quadratic models we computed the Bayesian information criterion (BIC), a metric that quantifies goodness of fit while accounting for the number of parameters included in the model. Results were compared using a Bayes Factor (BF).[34] In brief, BF is computed as follows:

$$BF_{QL} = exp(\Delta BIC_{LQ} / 2)$$

where ΔBIC_{LQ} is the difference in the BIC obtained for each model. QL indicates the evidence in favor of the quadratic (Q) over the linear (L) model and vice versa. This formulation is consistent with the "unit information prior". The BF quantifies the strength of the evidence for one model as compared to the other and can be interpreted according to standard guidelines.[35]

Topographies' correlation

Having observed a similar, significant frequency preference in both experiments in the 30° resolution, we sought to quantify the extent to which this similar response is expressed in the pattern of sensor level activity. To this end, we correlated the group-average topography of the ITC difference between frequencies tagged with 6- and 4-fold periodicity between the spatial (i.e., Figure 2C, right) and non-spatial experiment (i.e., Figure 5A, right) in the 30° resolution.

Moreover, we reasoned that a grid-like response should be relatively independent of the granularity of the space that is used in its investigation, thus providing a similar response pattern in both spatial resolutions that were tested in the current experiment.

To investigate this, we computed the (within-participant) similarity of the topographies of the grid-like effect (i.e., ITC_6 - ITC_4) between the 15° and 30° angular resolutions. We focused on 6- and 4-fold periodicities given that they were common between angular resolutions. Similarly, in the non-spatial experiment we computed the correlation of the topographies (ITC_{Cont6} - ITC_{Cont4}) between the conditions corresponding to the 15° and 30° resolutions. Correlation values were fisher transformed before further analysis. A one-sample t test was used to investigate whether the correlations at the group level were significantly different from zero. An independent samples t test was instead used to compare the correlation scores across experiments.